

# Deep Bayesian Supervised Learning given Hypercuboidally-shaped, Discontinuous Data, using Compound Tensor-Variate & Scalar-Variate Gaussian Processes

Kangrui Wang<sup>\*,†</sup>, Dalia Chakrabarty<sup>†,§</sup> ,

<sup>†</sup> *Department of Mathematics*

*University of Leicester*

*Leicester LE1 3RH, U.K.*

[kw2020@le.ac.uk](mailto:kw2020@le.ac.uk)

<sup>§</sup> *Department of Mathematical Sciences*

*Loughborough University*

*Loughborough LE11 3TU, U.K.*

[d.chakrabarty@lboro.ac.uk](mailto:d.chakrabarty@lboro.ac.uk)

**Abstract:** We undertake learning of the high-dimensional functional relationship between a system vector and an observable that is in general tensor-valued, where this observable bears influence on the system parameter. The ultimate aim is to undertake Bayesian inverse prediction of the system parameter vector, at which a new measurement on the observable is reported. We attempt such learning given hypercuboidally-shaped data comprising multiple measurements of the tensor-valued observable, where the data displays strong discontinuities, rendering learning challenging. We undertake modelling of the sought functional relationship, with a tensor-variate Gaussian Process (GP) and use three independent ways for learning the covariance matrices of the resulting likelihood which is Tensor-Normal. We demonstrate that when the covariance matrix is kernel parametrised, the discontinuous nature of the data demands the implemented kernel to be non-stationary, which we achieve by modelling each hyperparameter of the kernel, as a function of the sample function of the invoked tensor-variate GP. This translates to a dynamically varying function, within our Bayesian inference scheme—with this function treated as a realisation from a scalar-variate GP, the covariance structure of which is described adaptively by collating information from a historical set of samples. Parameters of this "inner-layer" comprising scalar-variate GPs, are updated first in our Metropolis-within-Gibbs scheme, thus allowing kernel hyperparameters to be updated; remaining parameters of the tensor-variate GP are then updated in the second block. Thus, the functional relation between the system parameter and observable is learnt, and subsequently, we perform inverse Bayesian prediction. We apply our method to a cuboidally-shaped, discontinuous, real dataset, while undertaking forward prediction to generate data from our model, given our results—to perform model-checking.

---

<sup>\*</sup>PhD student in Department of Mathematics, University of Leicester

<sup>†</sup>Lecturer in Statistics, Department of Mathematical Sciences, Loughborough University

**Keywords and phrases:** Tensor-variate Gaussian Processes, Kernel parametrisation, Deep learning, Metropolis-within-Gibbs

## 1. Introduction

Statistical modelling allows for the learning of the relationship between two variables, where the said relationship is responsible for generating the data available on the variables. Thus, let  $\mathbf{X}$  be a random variable that represents a behavioural or structural parameter of the system, and  $\mathbf{Y}$  is another variable that bears influence on  $\mathbf{X}$  s.t.  $\mathbf{Y} = \mathbf{f}(\mathbf{X})$ , where the functional relation  $\mathbf{f}(\cdot)$  that we seek to learn, is itself a random structure, endowed with information about the error made in predicting the values of  $\mathbf{Y}$  (or  $\mathbf{X}$ ) at which the noise-included measurement of  $\mathbf{X}$  (or  $\mathbf{Y}$ ) has been realised. Such a function can be modelled as a realisation from an adequately chosen stochastic process. In general, either of both variables could be tensor-valued, such that, data comprising measurements of either variable, is then shaped as a hypercuboid. Typically, the structure/behaviour of a system is parametrised using a set of scalar-valued parameters, (say  $d$  number of such parameters), which can, in principle be collated into a  $d$ -dimensional vector. Then  $\mathbf{X}$  is typically, the system parameter vector. The other, observed variable  $\mathbf{Y}$ , can be tensor-valued in general. There are hypercuboidally-shaped data that show up in real-world applications, (Barton and Fuhrmann, 1993; Bijma et al., 2005; Mardia and Goodall, 1993; Theobald and Wuttke, 2008; Werner et al., 2008). For example, in computer vision, the image of one person might be a matrix of dimensions  $a \times b$ , i.e. image with resolution of  $a$  pixels by  $b$  pixels. Then, repetition across  $n$  persons inflates the data to a cuboidally-shaped dataset. Examples of handling high-dimensional datasets within computer vision exist (Dryden et al., 2009; Fu, 2016; Pang et al., 2016; Qiang and Fei, 2011; Wang, 2011). In health care, the  $p$  number of health parameters of  $n$  patients, when charted across  $k$  time-points, again generates a high-dimensional data, which gets further enhanced, if the experiment involves tracking for changes across  $\ell$  groups of  $n$  patients each, where each such group is identified by the level of intervention (Chari, Coe, Vucic, Lockwood and Lam, 2010; Chari, Thu, Wilson, Lockwood, Lonergan, Coe, Malloff, Gazdar, Lam, 2010; Clarke et al., 2008; Fan, 2017; Oberg et al., 2015; Sarkar, 2015; Wang et al., 2015). Again, in ecological datasets, there could be  $n$  spatial locations at each of which,  $p$  traits of  $k$  species could be tracked, giving rise to a high-dimensional data (Dunstan et al., 2013; Leitao et al., 2015; Warton, 2011).

That we treated these groups as independent—or for that matter, even the variation in parameter values of any group across the  $k$  time points, is ignored, and a mere snapshot of each group is traditionally considered one at a time—is a shortcoming, of such traditional modelling strategies. In this work, we advance a method for the consideration of parameters across all relevant levels of measurement, within one integrated framework, to enable the learning of correlations across all such

levels, thus permitting the prediction of the system parameter vector, with meaningful uncertainties and avoid information loss associated with categorisation of data.

While discussing the generic methodology that helps address the problem of learning the inter-variable relationship  $f(\cdot)$ , given general hypercuboid-shaped data—comprising multiple measurements of the observable  $\mathbf{Y}$ , where each value of  $\mathbf{Y}$  is generated at a given value of the system parameter  $\mathbf{X}$ —we focus on developing such learning when this data displays discontinuities. In such a learning exercise, the functional relation  $f(\cdot)$  between the variables needs to be modelled using a high-dimensional stochastic process (a tensor-variate Gaussian Process, for example), the covariance function of which is non-stationary. The correlation between a pair of data slices, (defined by two such measured values of  $\mathbf{Y}$ , each realised at two distinct values of the system parameter  $\mathbf{X}$ ), is sometimes parametrically modelled as a function of the distance between the values of the system parameter at which these slices are realised, i.e. “similarity” in values of  $\mathbf{Y}$  can be modelled as a function of “similarity” in the corresponding  $\mathbf{X}$  values. However, if there are discontinuities in the data, then such a mapping between “similarities” in  $\mathbf{X}$  and  $\mathbf{Y}$  no longer holds. In other words, discontinuities in data call for a model of the correlation that adapts to the discontinuities in the data. We present such correlation modelling in this paper, by modelling each scalar-valued hyperparameter of the correlation structure of the high-dimensional stochastic process, as a random function of the sample path of that process; this random function then, can itself be modelled as a realisation of a scalar-variate stochastic process—a scalar-variate Gaussian Process (GP) for example. Thus, the learning of  $f(\cdot)$  is double-layered in which multiple scalar-variate GPs inform a high-dimensional (tensor-variate) GP. The data on the observable  $\mathbf{Y}$  can be shown to be sampled from a compound tensor-variate and multiple scalar-variate Gaussian Processes.

Acknowledgement of nonstationarity in correlation learning is not new (Paciorek and Schervish, 2004). In some approaches, a transformation of the space of the input variable is suggested, to accommodate non-stationarity (Sampson and Guttorp, 1992; Schmidt and OHagan, 2003; Snoek et al., 2014). When faced with learning the dynamically varying covariance structure of time-dependent data, others have resorted to learning such a covariance, using Generalised Wishart Process (Wilson and Ghahramani, 2011). In another approach, latent parameters that bear information on non-stationarity, have been modelled with GPs and learnt simultaneously with the sought function (Tolvanen et al., 2014), while others have used multiple GPs to capture the non-stationarity (Gramacy, 2005; Heinonen et al., 2016). However, what has not been presented, is a template for including non-stationarity in high-dimensional data, by nesting lower-dimensional Gaussian Processes with distinct covariances, within a tensor-variate GP (Section 2 and Section 3), using a Metropolis-within-Gibbs inference scheme (Section 4), to perform with-uncertainties learning of a high-dimensional function, given discontinuities that show up in the hypercuboidally-shaped datasets in general, and illustration of the method on a cuboidally-shaped, real-world dataset (Section 5, Section 6). This is what we introduce in this

paper. Our model is capacitated to learn the temporally-evolving covariance of time-dependent data, if such is the data at hand, but the focus of our interest is to follow the learning of the sought tensor-valued functional relation between a system parameter vector and a tensor-valued observable, with inverse Bayesian prediction of the system parameter values, at which test data on the observable is measured (Section 7, Section 6). Additionally, flexibility of our model design allows us to undertake both inverse and forward predictions. So we also predict new data at chosen system parameter values given our model and results, and perform model checking, by comparing such generated data against the empirically observed data (Section 8).

## 2. Model

Here the system parameter vector is  $\mathbf{X} \in \mathbb{R}^d$ . Let the observable  $\mathbf{Y}$  be tensor-valued in general, i.e.  $\mathbf{Y}$  a  $k-1$ -th ordered tensor-valued variable, i.e. is  $m_1 \times m_2 \times \dots \times m_{k-1}$ -dimensional, where  $m_i \in \mathbb{Z}, \forall i = 1, \dots, k-1$ . Then we write,  $\mathbf{Y} \in \mathcal{Y} \subseteq \mathbb{R}^{m_1 \times m_2 \times \dots \times m_{k-1}}$ .

Given this structure of  $\mathbf{Y}$ , and the relationship  $\mathbf{Y} = \mathbf{f}(\mathbf{X})$  between  $\mathbf{X}$  and  $\mathbf{Y}$ , we realise that the sought function  $\mathbf{f}(\cdot)$  is a map of the following nature;  $\mathbf{f} : \mathcal{X} \subseteq \mathbb{R}^d \xrightarrow{k-1} \mathcal{Y} \subseteq \mathbb{R}^{m_1 \times m_2 \times \dots \times m_{k-1}}$ , i.e.  $\mathbf{f}(\cdot)$  is itself a high-dimensional, or “tensor-valued function”, with  $\prod_{i=1}^{k-1} m_i$ -number of component functions, with these components suffering inter-correlations. Thus, the learning of  $\mathbf{f}(\cdot)$  is equivalent to learning the multiple functions, and such learning is inclusive of learning the correlation amongst these component functions.

If,  $k = 1$  and  $\mathbf{Y}$  is a vector  $\in \mathbb{R}^{m_1}$ , (say), then  $\mathbf{f}(\cdot)$  would be rendered a vector-valued function, i.e. a function with  $m_1$  number of component functions,  $f_1(\cdot), \dots, f_{m_1}(\cdot)$ , s.t. at  $\mathbf{X} = \mathbf{x}_i$ ,  $f_j(\mathbf{x}_i) = y_j^{(i)}, j = 1, \dots, m_1; i = 1, \dots, N$ , where the  $m_1$ -dimensional vector  $\mathbf{y}_i = (y_1^{(i)}, \dots, y_{m_1}^{(i)})^T$ , and the correlation amongst  $y_1^{(i)}, \dots, y_{m_1}^{(i)}$  is the same as that amongst  $f_1(\mathbf{x}_i), \dots, f_{m_1}(\mathbf{x}_i)$ . The inverse of this function  $\mathbf{f}(\cdot)$ , is the  $m_1$ -dimensional vector of the inverses of the component functions. In the conventional framework, to find value  $\mathbf{x}^{(new)}$  of the  $d$ -dimensional  $\mathbf{X}$ , at which a new (measured) value  $\mathbf{y}^{(new)}$  of  $\mathbf{Y}$  is realised, we compute:  $\mathbf{x}^{(new)} := \mathbf{f}^{-1}(\mathbf{Y})|_{\mathbf{Y}=\mathbf{y}^{(new)}}$ . Here, the  $m_1$ -dimensional vector  $\mathbf{y}^{(new)} := (y_1^{(new)}, \dots, y_{m_1}^{(new)})^T$ . Then for the above equation to offer solutions, we need  $d \leq m_1$ , and while the equation fundamentally represents an overdetermined system, s.t. unique solutions are not expected unless  $d = m_1$ , the learnt correlation amongst the  $m_1$ -number of component functions compensates for this over-determinedness, to allow for solutions that are consistent within the uncertainty levels at which each component of  $\mathbf{x}^{(new)}$  is Bayesianly inferred upon. The over-determinedness is not expected to always be exactly compensated by the learnt correlation structure, but in a Bayesian setting, the non-uniqueness of the solutions only contributes to inflating the 95% Highest Probability Density credible regions on the learnt function.

The inversion of the sought function  $\mathbf{f}(\cdot)$ —where  $\mathbf{Y} = \mathbf{f}(\mathbf{x})$ —allows for the forward prediction of

$\mathbf{y}^{(new)}$  given a measured value  $\mathbf{x}^{(new)}$  of  $\mathbf{X}$ , as well as for the inverse prediction of the value of  $\mathbf{X}$  at which a given measurement of  $\mathbf{Y}$  is recorded. However, if we had set ourselves the task of learning  $\mathbf{g}(\cdot)$ , where  $\mathbf{g}(\mathbf{Y}) = \mathbf{X}$ , i.e.  $\mathbf{g}(\cdot)$  is a “vector-valued” function in the jargon motivated above—and therefore lower dimensional with fewer number of component functions than the tensor-valued  $\mathbf{f}(\cdot)$ —we could not have performed the prediction of the value of  $\mathbf{Y}$  at a given  $\mathbf{x}$ . The vector-valued inverse of such a  $\mathbf{g}(\cdot)$  function (with  $d$  component functions) cannot yield a value of the  $\prod_{i=1}^{k-1} m_i$  number of components of the tensor  $\mathbf{Y}$  at this given  $\mathbf{X}$ , as long as  $\prod_{i=1}^{k-1} m_i > d$ . This is why we undertake the seemingly more difficult learning of the tensor-valued  $\mathbf{f}(\cdot)$  (that outputs the tensor  $\mathbf{Y}$ ), than the vector-valued  $\mathbf{g}(\cdot)$  (that outputs the vector  $\mathbf{X}$ ). After all, we want to retain the capacity of predicting both a new datum at a given value of the system parameter ( $\mathbf{X}$ ), as well as predict the system parameter at which a new measurement of the observable  $\mathbf{Y}$  is realised.

The Bayesian learning of the function  $\mathbf{f}(\cdot)$ , uses the training data  $\mathbf{D} := \{(\mathbf{x}_i, \mathbf{y}_i)\}_{i=1}^N$ . Above, we have referred to the conventional prediction of  $\mathbf{X} = \mathbf{x}^{(test)}$ , at which test datum  $\mathbf{y}^{(test)}$  on  $\mathbf{Y}$  is realised, as:  $\mathbf{x}^{(test)} := \mathbf{f}^{-1}(\mathbf{Y})|_{\mathbf{y}^{(test)}}$ . However, this formulation renders the learning of the uncertainty in the prediction difficult, and there is no objective way to include the uncertainties learnt in the learning of the function  $\mathbf{f}(\cdot)$ , to propagate into the uncertainty of this prediction. This underpins an advantage of Bayesian prediction of one variable, given test data on the other, subsequent to learning of  $\mathbf{f}(\cdot)$  using training data  $\mathbf{D}$ . Conventional fitting methods (such as fitting with splines, etc), fumble under multiple other realistic complications as well. The measured values of both/either of the r.v.s  $\mathbf{X}$  and  $\mathbf{Y}$ , can be accompanied by measurement errors; in light of this, it becomes difficult to infer the function that fits the data the best. In fact, the uncertainty in the learning of the sought function is also then difficult to quantify. Secondly, there is no organic suggestion as to what the smoothness of the sought  $\mathbf{f}(\cdot)$  should be. Ideally, we would prefer to learn this smoothness from the data itself. However, there is nothing intrinsic to the fitting-with-splines/wavelets method that can in principle, quantify the smoothness of the curve, given a training data. Lastly, when  $\mathbf{Y}$  is an r.v. that is no longer a scalar, but higher-dimensional (say tensor-valued in general), fitting with splines/wavelets starts to become useless, since in such cases of sought tensor-valued function  $\mathbf{f}(\cdot)$  (in general), the component functions of  $\mathbf{f}(\cdot)$  are correlated, but methods such as parametric fitting approaches, cannot capture such correlation, given the training data. As we have remarked above, such correlation amongst the components functions of  $\mathbf{f}(\cdot)$  is the same correlation structure amongst the components of the tensor-valued  $\mathbf{Y}$ —so in principle, the sought correlation can be learnt from the training data.

In light of this, we identify a relevant Stochastic Process that can give a general, non-restrictive description of the sought function  $\mathbf{f}(\cdot)$ —a Gaussian Process for example. The joint probability density of a set of realisations of a sampled  $\mathbf{f}(\cdot)$ , is then driven by the Process under considerations, where

each such realisation of the function, equals a value of the output variable  $\mathbf{Y}$ . Thus, the joint also represents the likelihood of the Process parameters given the relevant set of values of  $\mathbf{Y}$ , i.e. the data. We impose judiciously chosen priors, to write the posterior probability density of the Process parameters given the data. Generating samples from this posterior then allows for the identification of the 95% HPD credible regions on these Process parameters, i.e. on the learnt function  $\mathbf{f}(\cdot)$ . It is possible to learn the smoothness of the function generated from this Process, via kernel-based parameterisation of the covariance structure of the GP under consideration. Thus, we focus on the pursuit of adequate covariance kernel parametrisation.

Importantly, we model some covariance matrices using a kernel parametrisation technique that allows for the potently simple—though unrealistic—assumption of stationarity to be included in the global structure of the covariance matrix, while then allowing for the modelling of each parameter of such a simplistic kernel using an independent, scalar-variate Gaussian Process. This then effectively counters the original stationarity of the model, and renders the covariance structure realistic given the expected discontinuities in real-life datasets.

### 2.1. Method

In this section, we discuss a method of learning the tensor-valued functional relation  $\xi(\cdot)$  between  $d$ -dimensional system parameter vector  $\mathbf{S}$  and the  $k - 1$ -th ordered tensor-valued observable  $\mathbf{V}$  that affects  $\mathbf{S}$ , i.e.  $\mathbf{V} = \xi(\mathbf{S})$ . We model  $\xi(\cdot)$  as a realisation from a tensor-variate GP. Then, joint probability of the set of  $n$  realisations of the sampled function  $\xi(\cdot)$  at each of the  $n$  design points  $\mathbf{s}_1, \dots, \mathbf{s}_n$  (that reside within the training data  $\mathbf{D} = \{(\mathbf{s}_i, \mathbf{v}_i)\}_{i=1}^n$ ), follows the  $k$ -variate Tensor Normal distribution (Kolda and Bader, 2009; Manceur and Dutilleul, 2013; McCullagh, 1987; Richter et al., 2008), i.e. modelling of  $\xi(\cdot)$  with this tensor-variate GP implies that the joint probability distribution  $[\xi(\mathbf{s}_1), \dots, \xi(\mathbf{s}_n)] \sim \mathcal{TN}(\mathbf{M}, \Sigma_1, \dots, \Sigma_k)$ . The covariance tensor of this  $k$ -th order Tensor Normal distribution, has been decomposed into  $k$  different covariance matrices by Tucker decomposition, (Hoff et al., 2011; Kolda and Bader, 2009; Manceur and Dutilleul, 2013; Xu and Yan, 2015), to yield the  $k$  number of covariance matrices,  $\Sigma_1, \dots, \Sigma_k$ , where the  $j$ -th covariance matrix  $\Sigma_j$  is an  $m_j \times m_j$ -dimensional square matrix,  $j = 1, \dots, k$ . The mean of this density is a  $k$ -th ordered mean tensor  $\mathbf{M}$  of dimensions  $m_1 \times \dots \times m_k$ . As Hoff (1997); Manceur and Dutilleul (2013) suggest, a  $k$ -th ordered random tensor  $\Sigma \in R^{m_1 \times m_2 \dots \times m_k}$  can be decomposed to a  $k$ -th ordered tensor  $\mathbf{Z}$  and  $k$  number of covariance matrices  $\Sigma_1, \dots, \Sigma_k$  by Tucker product, according to  $\Sigma = \mathbf{Z} \times_1 \Sigma_1 \times_2 \Sigma_2 \dots \times_k \Sigma_k$ . It can be proved that all tensors can be decomposed into a set of covariance matrices (Xu et al., 2011), though not uniquely. This may cause difficulty in finding the correct combination of covariance matrices that present the correlation structure of the data at hand. One way to solve this problem is to use priors for the respective covariance parameters.

By virtue of  $\mathbf{V} = \xi(\mathbf{S})$ , it then follows that the joint of  $\mathbf{v}_1, \dots, \mathbf{v}_n$  is Tensor Normal, i.e.

$$[\mathbf{v}_1, \dots, \mathbf{v}_n] \sim \mathcal{TN}(\mathbf{M}, \Sigma_1, \dots, \Sigma_k),$$

i.e. likelihood of  $\mathbf{M}, \Sigma_1, \dots, \Sigma_k$  given  $\mathbf{D}$  is a Tensor Normal density:

$$\ell(\mathbf{M}, \Sigma_1, \dots, \Sigma_k | \mathbf{D}) \propto \exp(-\|(\mathbf{D}_V - \mathbf{M}) \times_1 \mathbf{A}_1^{-1} \times_2 \mathbf{A}_2^{-1} \dots \times_k \mathbf{A}_k^{-1}\|^2/2), \quad (2.1)$$

where  $n$  observed values of the  $k-1$ -th ordered tensor-valued variable  $\mathbf{V}$  are collated to form the  $k$ -th ordered tensor  $\mathbf{D}_V$ . The notation  $\times_j$  in Equation 2.1 presents the  $j$ -mode product of a matrix and a tensor (Oseledets, 2011). Here the  $j$ -th covariance matrix  $\Sigma_j = \mathbf{A}_j \mathbf{A}_j^T, j = 1, \dots, k$ , i.e. i.e.  $\mathbf{A}_j$  is the unique square-root of the positive definite covariance matrix  $\Sigma_j$ . One example of a computational algorithm that can be invoked to realise such a square root of a matrix, is Cholesky decomposition.

We employ this likelihood in Equation 2.1 to write the joint posterior probability density of the mean tensor and covariance matrices, given the data. But prior to doing that, we identify those parameters—if any—that can be estimated in a pre-processing stage of the inference, in order to reduce the computational burden of inference. Also, it would be useful to find ways of (kernel-based) parametrisation of the sought covariance matrices, thereby reducing the number of parameters that we need to learn. To this effect, we undertake the estimation of the mean tensor is  $\mathbf{M} \in R^{m_1 \times m_2 \dots \times m_k}$ . It is estimated as the sample mean  $\bar{\mathbf{v}}$  of the sample  $\{\mathbf{v}_1, \dots, \mathbf{v}_n\}$ , s.t.  $n$  repetitions of  $\bar{\mathbf{v}}$  form the value  $\mathbf{m}$  of  $\mathbf{M}$ . Then once  $\mathbf{m}$  is removed from the data  $\mathbf{D}_V$ , the data can be modelled with a zero-mean  $k$ -th ordered tensor-variate GP. However, if necessary, the mean tensor itself can be regarded as a random variable and learnt from the data (Chakrabarty et al., 2015). The modelling of the covariance structure of this GP is discussed in the following subsection.

Ultimately, we want to predict the value of one variable, at which a new or test data on the other variable is observed. So when it comes to the inverse prediction of the value  $\mathbf{s}^{(test)}$  of the input variable  $\mathbf{S}$ , at which test data  $\mathbf{v}^{(test)}$  on  $\mathbf{V}$  is realised, we can use two approaches. Under one, we sample from the posterior probability density of  $\mathbf{S}$  given the test data  $\mathbf{v}^{(test)}$ , and the tensor-valued parameters of the  $k$ -th ordered tensor-variate GP invoked to model  $\xi(\cdot)$ —learnt using the training data. Another is to write the joint posterior probability density of  $\mathbf{s}^{(test)}$  and all other parameters of this tensor-variate GP given training data, as well as test data, and sample from this joint posterior density using MCMC, for the 95% HPDs on  $\mathbf{s}^{(test)}$ . For large data sets, the two methods will give similar results. Since the marginal distribution for the GP parameters are learnt separately, the computational speed of the first approach, is much higher. When the training data is small, or if the training data is not representative of the test data at hand, the learning of  $\mathbf{s}^{(test)}$  via the second method may affect the learning of the GP parameters.

## 2.2. Different ways of learning covariance matrices

The total number of distinct parameters in the (symmetric)  $j$ -th covariance matrix that is  $m_j \times m_j$ -dimensional, is  $\frac{(m_j + 1) \times m_j}{2}$ . So if all the scalar components of all the  $k$  covariance matrices were to be learnt directly by MCMC, we could end up learning a very large number of parameters indeed, with the number of sought parameters increasing quadratically with both dimensionality of the data tensor and size of the dataset. This will imply an unaffordable calculating time. We can in principle learn all the covariance matrices directly, given the data. Hoff (1997) discusses the implementation of a maximum likelihood estimation technique to estimate the covariance matrices of such a tensor-variate GP. Alternatively, we advance an empirical estimation of  $\Sigma_j$  by collapsing each of the  $m_j$  number of high-dimensional ( $k - 1$ -th ordered tensor-shaped) slices of the data, along all-but-one axis in the native space of  $\mathbf{V}$ , i.e. along the  $j$ -th axis in this space. Such an operation then reduces each of the high-dimensional  $m_j$  slices to a vector. The covariance computed using a pair of such vectors (adjusted for sample size), is then an element of  $\Sigma_j$ . Each such reduced vector then possesses the compressed information from all the relevant dimensions of the data. The covariance matrix  $\Sigma_j$  is thus approximated by an empirical estimate of the covariance amongst such vectors. Indeed such an empirical estimate of any covariance matrix may then be easily generated, but it indulges in linearisation amongst the different dimensionalities of the observable  $\mathbf{V}$ , causing loss of information about the covariance structure amongst the components of these high-dimensional slices. This is however an approach that is inadequate when the sample size is small because the sample-based estimate will tend to be incorrect; indeed discontinuities and steep gradients in the data, especially in small-sample and high-dimensional data, will render such estimates of the covariance structure incorrect representation of the correlation structure of such data. Importantly, such an approach does not leave any scope for identifying the smoothness in the function  $\xi(\cdot)$  that represents the functional relationship between the input and output variables. Lastly, the uncertainties in the estimated covariance structure of the GP remain inadequately known.

Instead, we learn the covariance structure of the GP whenever we can, using Bayesian inference that allows for learning inclusive of uncertainties (as the 95% HPDs). Our employment of kernel parametrisation techniques, when possible, reduces the number of parameters in the covariance matrix thus parametrised, and also allows for an organic learning of the smoothing length scales of the function  $\xi(\cdot)$  sampled from the high-dimensional GP. Lastly, our Bayesian framework allows us to use priors for the covariance matrices. Kernel functions are usually distance based. Thus, the function itself, together with the distance observations, will bring in the information about the covariance structure.

For the  $p$ -th covariance matrix, let the  $ij$ -th element be  $\sigma_{ij}^{(p)}$ , i.e.  $\Sigma_p = [\sigma_{ij}]$ , where  $\Sigma_p$  is  $m_p \times m_p$ -dimensional, so that  $j, i = 1, \dots, m_p$ . Then  $\sigma_{ij}^{(p)}$  bears information about the covariance amongst the  $i$ -th and  $j$ -th slices of the data, where the data  $\mathbf{D}_V$  being a  $k$ -th ordered tensor, such

$i$ -th and  $j$ -th “slice” is each shaped like a  $k - 1$ -th ordered tensor. Here the  $i$ -th “slice” of the data is the value  $\mathbf{v}_i$  of  $\mathbf{V}$  that is realised at the  $i$ -th design point  $\mathbf{s}_i$ . Similarly, the  $j$ -th slice is  $\mathbf{v}_j$  that is realised at the value  $\mathbf{s}_j$  of the input variable  $\mathbf{S}$ .

The correlation—and therefore, the covariance  $\sigma_{ij}^{(p)}$ —between the  $i$ -th and  $j$ -th slices of the data then decreases as the slices get increasingly more disparate, where this disparity can be treated as increasing, with increasing difference in the values of  $\mathbf{S}$  at which these slices are realised, i.e. with increasing  $\| \mathbf{s}_i - \mathbf{s}_j \|$ . In fact, we can model the correlation  $\sigma_{ij}^{(p)}$  between the  $i$ -th and  $j$ -th slices of the data as a decreasing function of this disparity  $\| \mathbf{s}_i - \mathbf{s}_j \|$ . In an even more generalised model,  $\sigma_{ij}^{(p)}$  may be modelled as a decreasing function of some components of  $\mathbf{s}_i - \mathbf{s}_j$ , but trending differently with other components of  $\mathbf{s}_i$  and  $\mathbf{s}_j$ , where  $\mathbf{S}$  is a higher-dimensional than a scalar. In either modelling strategy, we suggest that  $\sigma_{ij}^{(p)}$  be modelled as a function  $K(\mathbf{s}_i, \mathbf{s}_j)$ . So in general, we can then define  $\sigma_{ij}^{(p)} = K_p(\mathbf{s}_i, \mathbf{s}_j)$ , where  $K_p(\mathbf{s}_i, \mathbf{s}_j)$  is the kernel function  $K_p(\cdot, \cdot)$ , computed at the  $i$ -th and  $j$ -th input variables. Thus, the number of distinct unknown parameters involved in the learning of  $\Sigma_p$  reduces from  $m_p(m_p + 1)/2$ , to the number of hyper-parameters that parametrise the kernel function  $K_p(\cdot, \cdot)$ .

However, kernel parametrisation is not always possible. There are two situations when we clearly cannot use kernel parametrisation. Firstly, this parametrisation may cause information loss and this may not be acceptable (Aston and Kirch, 2012). One example of this occurs when one uses stationary kernel to model the covariance structure of non-stationary data. Although this can be solved by changing into an appropriate, non-stationary kernel function, condensing all the information of the covariance matrix through such parametrisation may not be necessarily be lossless; so ideally, one may wish to learn each element of the covariance matrix directly (perhaps using MCMC, to gain the advantage of comprehensive 95% HPDs). Another situation when we will necessarily avoid kernel parametrisation of a covariance matrix, is when we cannot find input parameters, at which the corresponding slices in the data are realised, where the covariance matrix in question is composed of elements that are each, the pairwise covariance between a pair of such slices.

In such situations, we will learn the elements of the covariance matrix directly using MCMC. However, as discussed above, this can entail the learning of an infeasibly large number of parameters. So a direct learning of all distinct elements of  $\Sigma_p$  is feasible, as long as total number of all unknowns learnt by MCMC  $\lesssim 200$ . Alternatively, we can use an empirical estimation for the covariance matrix, as described above. In summary, we model the covariance matrices as kernel parametrised, or empirically-estimated, or learnt directly using MCMC. An accompanying computational worry is the inversion of any of the covariance matrices; for a covariance matrix that is an  $m_p \times m_p$ -dimensional matrix, the computational order for matrix inversion is well known to be  $O(m_p^3)$  (Knuth, 1997).

### 3. Kernel parametrisation

Often, including in our first application, a simple stationary covariance kernel, such as the Squared Exponential (SQE) covariance kernel, is used. The SQE kernel computed at two values  $\mathbf{s}_i$  and  $\mathbf{s}_j$  of the input space variable  $\mathbf{S}$ , depends on the Euclidean distance between  $\mathbf{s}_i$  and  $\mathbf{s}_j$  as:

$$K(\mathbf{s}_i, \mathbf{s}_j) = a_{ij} \exp(-(\mathbf{s}_i - \mathbf{s}_j)^T \mathbf{Q}^{-1}(\mathbf{s}_i - \mathbf{s}_j)) \quad (3.1)$$

where  $\mathbf{Q}$  is a diagonal matrix, the diagonal elements of which are the unknown length scale parameters that bear information about the extent in input space, over which correlations persist, i.e. these length scale parameters  $\ell_1, \dots, \ell_d$  tell us how quickly the correlation fades away along a given direction in the input space  $\mathcal{S}$ , i.e. the space of the  $d$ -dimensional vector-valued input variable  $\mathbf{S}$ . Then the matrix  $\mathbf{Q}^{-1}$  is the inverse of the diagonal matrix of the length scales, and is therefore diagonal itself, with the diagonal elements given as  $\frac{1}{\ell_1}, \dots, \frac{1}{\ell_d}$ , where we interpret  $1/\ell_q$  as the smoothness parameter, given that it is the reciprocal of the length scale parameter  $\ell_q$ ;  $q = 1, \dots, d$ . We learn these  $d$  unknown parameters from the data, using MCMC; indeed, these are treated as the hyperparameters of the covariance kernel. Here  $a_{ij}$  is the amplitude of the covariance matrix. We can learn all the  $a_{ij}$  parameters directly from MCMC. However, this will amount to a very large of parameters of the covariance matrix that we will then need to make inference upon. To avoid this, we interpret the SQE kernel parametrisation to be endowed a global scale instead, while the length scale parameters are unknowns that are learnt from the data. The resulting covariance structure then crucially depends on the distance between the pair of values of the input variable  $\mathbf{S}$  that the kernel is computed at:

$$K(\mathbf{s}_i, \mathbf{s}_j) := A \left[ \exp(-(\mathbf{s}_i - \mathbf{s}_j)^T \mathbf{Q}^{-1}(\mathbf{s}_i - \mathbf{s}_j)) \right],$$

where  $A$  is a global scale. An interpretation of this is that we have scaled all local amplitudes  $a_{ij}$  to be  $< 1$  using the global factor  $A$ , and these scaled local amplitudes are then subsumed into the argument of the exponential in the RHS of the last equation, s.t. the reciprocal of the correlation length scales, that are originally interpreted as the elements of the diagonal matrix  $\mathbf{Q}^{-1}$ , are now interpreted as the smoothing parameters modulated by such local amplitudes. The global scale  $A$  is itself subsumed as a scale factor, in one of the covariance matrices of the tensor-normal distribution at hand—this is the matrix, the distinct elements of which are learnt directly using MCMC, i.e. without resorting to any parametrisation or to any form of empirical estimation. If we do not use any empirical estimation or do not have any covariance matrices learnt directly, we can still learn this parameter using MCMC. However, it has to be kept in mind that the above interpretation is only loose, since the same smoothness parameters cannot accommodate all (scaled by a global factor) local amplitudes  $\in (0, 1]$ , for all  $\mathbf{s}_i - \mathbf{s}_j$ . This is why, our definition of the kernel function  $K(\mathbf{s}_i, \mathbf{s}_j)$  as in Equation 3 is best understood as our choice of model for the covariance kernel.

### 3.1. Imposing non-stationarity by modelling hyperparameters of covariance kernels as realisations of Stochastic Process

In our definition of the kernel function that we employ to parametrically model a covariance matrix  $\Sigma_p^{(m_p \times m_p)}$ , we have included a hyperparameter in the form of a smoothing parameter (reciprocal of the correlation length scale), and a global amplitude. These hyperparameters are unknowns, that we learn from the data. Then by definition of this kernel function, (Equation 3), all sample paths are endowed with the same length scale parameters  $\ell_1, \dots, \ell_d$ , and global amplitude  $A$ —each with the 95% HPD uncertainty that its MCMC-based learning entails. However, the data on the output variable  $\mathbf{V}$  is not continuous, defining the correlation between  $\xi(\mathbf{s}_i)$  and  $\xi(\mathbf{s}_j)$ , as dependent on the Euclidean distance  $\|\mathbf{s}_i - \mathbf{s}_j\|$  between them, will be an incorrect representation of the correlation at these two points in the input space. Indeed, then a stationary definition of the correlation for all pairs of points in the function domain, is wrong. One way to generalise the model for the covariance kernel is to suggest that the hyperparameters vary as random functions of the sample path.

**Theorem 3.1.** *For  $\mathbf{S} \in \mathcal{X}$  and  $\mathbf{V} \in \mathcal{Y}$ , the map  $\xi : \mathcal{X} \rightarrow \mathcal{Y}$  is a Lipschitz-continuous map, if correlation between  $\xi(\mathbf{s}_1)$  and  $\xi(\mathbf{s}_2)$  is s.t.*

$$\text{corr}(\xi(\mathbf{s}_1) - \xi(\mathbf{s}_2)) := K(\langle (\mathbf{s}_1 - \mathbf{s}_2), \mathbf{q} \rangle^2), \quad \forall \mathbf{s}_1, \mathbf{s}_2 \in \mathcal{X},$$

where

$$K(\mathbf{s}_1, \mathbf{s}_2) := \exp\left[-\frac{\langle (\mathbf{s}_1 - \mathbf{s}_2), \mathbf{q} \rangle^2}{2}\right]$$

and each element of the vector  $\mathbf{q}$  of correlation hyperparameters is  $\xi$ -dependent, i.e.

$$\mathbf{q}(\xi) = (q_1(\xi), \dots, q_d(\xi))^T \in \mathbb{R}^d.$$

*Proof.* For  $\mathbf{S} \in \mathcal{X}$  and  $\mathbf{V} \in \mathcal{Y}$ , the mapping  $\xi : \mathcal{X} \rightarrow \mathcal{Y}$  is defined to be Lipschitz-continuous map, if

$$d_{\mathcal{Y}}(\xi(\mathbf{s}_1) - \xi(\mathbf{s}_2)) \leq L_{\xi} d_{\mathcal{X}}(\mathbf{s}_1, \mathbf{s}_2), \quad \forall \mathbf{s}_1, \mathbf{s}_2 \in \mathcal{X},$$

—for constant  $L_{\xi} \in \mathbb{R}$ , s.t. the infimum over all such constants is the Lipschitz constant for  $\xi$ ;

— $(\mathcal{X}, d_{\mathcal{X}})$  and  $(\mathcal{Y}, d_{\mathcal{Y}})$  are metric spaces.

Then defining the metric  $d_{\mathcal{X}}(\xi(\cdot, \cdot))$  as the usual Euclidean distance:

$$d_{\mathcal{X}}(\mathbf{s}_1, \mathbf{s}_2) := \|\mathbf{s}_1 - \mathbf{s}_2\|, \quad \forall \mathbf{s}_1, \mathbf{s}_2 \in \mathcal{X},$$

and the metric  $d_{\mathcal{Y}}(\xi(\cdot, \cdot))$  as:

$$d_{\mathcal{Y}}(\xi(\mathbf{s}_1), \xi(\mathbf{s}_2)) := -\log(\text{corr}(\xi(\mathbf{s}_1), \xi(\mathbf{s}_2))), \quad \forall \mathbf{s}_1, \mathbf{s}_2 \in \mathcal{X},$$

where correlation between functional values being a measure of affinity that lies in  $[-1, 1]$ , the transformation  $(\log(1/\text{corr}(\cdot, \cdot)))$  to the non-negative metric is undertaken.

Here the correlation is modelled using an SQE-looking form:

$$\text{corr}(\xi(s_1), \xi(s_2)) := \exp[-\langle (s_1 - s_2), \mathbf{q} \rangle^2], \quad \forall s_1, s_2 \in \mathcal{X}, \mathbf{q} \in \mathbb{R}^d,$$

so that we find

$$d_{\mathcal{Y}}(\xi(s_1), \xi(s_2)) = \langle (s_1 - s_2), \mathbf{q} \rangle^2.$$

Then for the map  $\xi$  to be Lipschitz-continuous, we require:

$$\sum_{i=1}^d q_i^2 (s_1^{(i)} - s_2^{(i)})^2 \leq L_{\xi} \sum_{i=1}^d (s_1^{(i)} - s_2^{(i)})^2,$$

where the vector of correlation hyperparameters is  $\mathbf{q} = (q_1, \dots, q_d)^T$ .

By choosing to define  $q_{\max} := \max(q_1, \dots, q_d)$ , and

$$(q_i')^2 := \left( \frac{q_i}{q_{\max}} \right)^2 \leq 1, \forall i = 1, \dots, d$$

, the above requirement is met, if we choose the  $\xi$ -dependent Lipschitz constant  $L_{\xi}$  to be:

$$L_{\xi} = q_{\max}^2,$$

i.e. the map  $\xi$  is Lipschitz-continuous, if  $q_{\max}$  is  $\xi$ -dependent, and therefore, in the definition of the distance  $\mathbf{Y}$  above (and therefore in the definition of its corresponding affinity measure, i.e. in correlation), the correlation hyperparameter  $q_i$  is  $\xi$ -dependent,  $\forall i = 1, \dots, d$ .  $\square$

**Remark 3.1.** *Above,  $q_1, \dots, q_d$  are hyperparameters of the correlation kernel; they are interpreted as the reciprocals of the length-scales  $\ell_1, \dots, \ell_d$ , i.e.  $\ell_i = 1/q_i, \forall i = 1, \dots, d$ .*

**Remark 3.2.** *Theorem 3.1 urges relaxation on the restriction of a universal correlation length scale in all sampled functions  $\xi(\cdot)$ , to ensure Lipschitz continuity of the map from the metric space  $\mathcal{X}$  to  $\mathcal{Y}$ . As any Lipschitz continuous function is also uniformly continuous, setting length scale hyperparameters (or their reciprocals) as varying with the sampled function, covers for discontinuities introduced via the data that the sampled function models.*

We update our original model for the covariance kernel, to one in which the hyperparameters are themselves randomly varying with the sample path, or rather the function  $\mathbf{x}(\cdot)$  that is sampled from the tensor-variate GP. In the Metropolis-within-Gibbs-based inference that we undertake, there is one sample function of the tensor-variate GP realised, in every iteration of the  $t_{\max}$  number of iterations long chain that we employ, (iteration number  $t = 1, \dots, t_{\max}$ ). Thus, the kerne hyperparameter along the direction  $c$  in the space of the input variable  $\mathbf{S}$ , that we model as varying with the sample path of the tensor-variate GP, is equivalently, varying with the iteration number  $t$ . (To clarify, it is only the correlation length scale hyperparameters  $\ell_1, \dots, \ell_d$  that we model in this way, given that the global amplitude  $A$  is subsumed as a scale into that covariance matrix that is learnt directly

using MCMC). Thus, the proposed model at this point of our model-building strategy is  $\ell_c = g_c(t)$ , where  $g_c : \mathbb{Z}_{>0} \rightarrow \mathbb{R}_{\geq 0}$ ,  $c = 1, \dots, d$  and this scalar-valued random function  $g_c(\cdot)$  is a realisation of a scalar-variate GP. The invoked scalar-variate GP that  $g_c(\cdot)$  is sampled from, is independent of the GP that  $g_{c'}(\cdot)$  is sampled from;  $c \neq c'; c, c' = 1, \dots, d$ .

In addition, we propose treating each scalar-valued function  $g_c(t)$  as distinct for distinct values of some descriptor variables that we choose to model this function with, where such descriptor parameters are themselves random, i.e. we obtain different output from the function  $g_c(t)$ , for one value of the descriptor variable vector  $\mathbf{X}$ , than for another value of  $\mathbf{X}$ . This dependence then needs to be reflected in the notational representation of the functional relation between iteration number and  $\ell_c$ . We achieve this, by suggesting:  $\ell_c = g_{c,\mathbf{x}}(t)$ , where  $g_c(\cdot)$  is a realisation of a scalar-variate GP. Here, the vector  $b\mathbf{X}$  that comprises the chosen descriptor variables where such a scalar-valued function is indexed by the sample path of the tensor-variate GP. We refer to our chosen vector of descriptor variables as  $\mathbf{X}$ ; we choose 2 such descriptor variables: the amplitude variable that takes the value  $a \geq 0$ , and a scale variable that takes the value  $\delta \in \mathbb{R}$ . Thus,  $\mathbf{x} = (a, \delta)$  and  $\mathbf{X} \in \mathcal{X} \subseteq \mathbb{R}^2$ . The underlying principle then is to sample a new value of the correlation length scale parameter of the kernel that parametrises a covariance matrix of the tensor-normal likelihood, at every new sample of the tensor-valued function  $\xi(\cdot)$  (from the Tensor Normal GP).

Thus our length scale parameter  $\ell_c$  in the  $c$ -th direction of the native space of  $\mathbf{S}$ , is a random, scalar-valued function  $g_{c,\mathbf{x}}(t)$  of time, labelled by the descriptor variables:  $a, \delta$ . In our modelling strategy, let us decide to acknowledge the effect of only the past  $t_0$  number of iterations on the current, i.e. the  $t$ -th iteration. Thus, we set the correlation length scale in the  $c$ -th direction in the input space of function  $\xi(\cdot)$ , to be:

$$\begin{aligned} \ell_c &= g_{c,\mathbf{x}}(t - t'), \quad \text{if } t \geq t_0, \quad c = 1, \dots, d; t' = 1, \dots, t_0, \\ \ell_c &= \ell_c^{(const)}, \quad \text{if } t = 0, 1, \dots, t_0 - 1, \quad c = 1, \dots, d, \end{aligned} \quad (3.2)$$

where  $\ell_c^{(const)}$  is an unknown constant that we learn from the data, during the first  $t_0$  iterations, for  $c = 1, \dots, d$ , i.e. for the first  $t_0$  iterations, the length scale parameter is not dynamically varying. At the current iteration, with number  $t \geq t_0$ , we model the scalar-valued functional relationship between the length scale parameter along the  $c$ -th direction of the space of the input variable  $\mathbf{S}$ , and time, or rather iteration number, as a realisation from a scalar-variate GP, s.t. the joint probability distribution of  $t_0$  number of values of the function  $g_{c,\mathbf{x}}(t)$ —each at a distinct  $\mathbf{x} = (a, \delta)^T$ —is Multivariate Normal, with a  $t_0$ -dimensional mean vector  $\mathbf{M}_{c,\mathbf{x}}$  and a  $t_0 \times t_0$ -dimensional covariance matrix  $\mathbf{\Psi}_{c,\mathbf{x}}$ , i.e.

$$[g_{c,\mathbf{x}}(t - 1), \dots, g_{c,\mathbf{x}}(t - 2), g_{c,\mathbf{x}}(t - t_0)] \sim \mathcal{MN}(\mathbf{M}_{c,\mathbf{x}}, \mathbf{\Psi}_{c,\mathbf{x}}). \quad (3.3)$$

Here  $t_0$  is the number of iterations that we look back at, to collect the dynamically-varying “look back-data”  $\mathbf{D}_{c',t} := \{\ell_c^{(t-t_0)}, \dots, \ell_c^{(t-1)}\}$  that is employed to learn parameters of the scalar-variate

GP that  $g_{c,\mathbf{x}}(\cdot)$  is modelled with. There is no data-driven constraint on the choice for the number  $t_0$  that gives the sample size of the realisations of each of the  $d$  length scale parameters. On the other hand, the value of  $t_0$  is driven to ensure feasibility of computation, since dimensionalities of  $\mathbf{M}_{c,\mathbf{x}}$  and  $\Psi_{c,\mathbf{x}}$  are affected by  $t_0$ .

The  $t_0$ -dimensional mean vector  $\mathbf{M}_{c,\mathbf{x}}$  is the empirical estimate of the mean of the dynamically varying look back-data, and so, at the  $t$ -th iteration it takes an estimated value  $m_{c,\mathbf{x}} := [\ell_{c,t-t_0} + \dots + \ell_{c,t-1}]/t_0$ , i.e. the empirical mean of the realisations of the  $c$ -th length scale in the  $t-1$ -th iteration, to the  $t-t_0$ -th iteration. Thus, computational load is not affected by  $t_0$  as far as this mean vector is concerned. In fact, in the  $t$ -th iteration, upon the empirical estimation of the mean as given above, it is subtracted from the “look back-data”  $\mathbf{D}_{c',t}$  so that the subsequent mean-subtracted look back-data  $\mathbf{D}_{c,t} := \{\ell_{c,t-t_0} - m_{c,t}, \dots, \ell_{c,t-1} - m_{c,t}\}$ . It is indeed this mean-subtracted sample that we use. Thus, the likelihood, or the joint probability of the  $t_0$  elements of this dataset  $\mathbf{D}_{c,t}$ , is Multivariate Normal with mean vector  $\mathbf{0}$  and covariance matrix  $\Psi_{c,\mathbf{x}}$ , ( $\forall c = 1, \dots, d$ , where  $d$  is the dimensionality of the input variable  $\mathbf{S}$  in the definition of the original learning problem:  $\mathbf{V} = \xi(\mathbf{S})$ ).

**Theorem 3.2.** *The dynamically varying covariance matrix of the Multivariate Normal likelihood in Equation 3.3, at iteration number  $t \geq t_0$ , is*

$$\Psi(t) \sim \mathcal{GWP}(d, \mathbf{G}, k(\cdot, \cdot)),$$

where the number of iterations we look back to is  $t_0$ ;  $\mathbf{G}$  is a scale matrix that contains the amplitudes of the  $k(\cdot, \cdot)$  covariance functions of the scalar-variate GP that generates the scalar-valued functional relation  $g_{c,\mathbf{x}}(t)$  that is equal to the  $c$ -th correlation length scale hyperparameter  $\ell_c$ , of the kernel-parametrised covariance matrix of the Tensor-Normal joint probability density of the training data  $\mathbf{D}$  that is employed to learn the tensor-valued functional relation between  $d$ -dimensional system parameter vector  $\mathbf{S}$  and tensor-valued observable  $\mathbf{V}$ . Here  $c = 1, \dots, d$  and the value of the vector of descriptor variables is  $\mathbf{x} = (a, \delta)$ , where  $a$  is the value of the amplitude variable and  $\delta$  the scale-length used in the definition of the covariance function of the scalar-variate GP, for each  $c = 1, \dots, d$ .

*Proof.* The covariance matrix  $\Psi_{c,\mathbf{x}}$  of the Multivariate Normal likelihood in Equation 3.3, at  $t \geq t_0$ ,  $\Psi_{c,t} = [k_{c,\mathbf{x}}(t - t_i, t - t_j)]$ ,  $i, j = 1, \dots, t_0$ . We hold  $k_{c,t}(\cdot, \cdot)$  to be independent of the input space direction and the iteration, i.e. the kernel parametrisation of the correlation does not vary with either input space direction, or iteration number. Thus, this kernel is designated  $k(\mathbf{x}_i, \mathbf{x}_j)$ . Then –as long as we set  $k(\mathbf{x}_i, \mathbf{x}_i) = 1 \forall i = 1, \dots, t_0$ ; –define the vector of functions  $\mathbf{g}_c(t) = (g_{c,\mathbf{x}_1}(t), \dots, g_{c,\mathbf{x}_{t_0}}(t))^T$ ; –invoke the positive definite square scale matrix  $\mathbf{G}$  of dimensionality  $t_0$ , containing the amplitudes of the  $k(\cdot, \cdot)$  functions,

at a given iteration number  $t$ , the r.v.  $\Psi(t) := \sum_{c=1}^d \mathbf{L}_G \mathbf{g}_c(t) \mathbf{g}_c^T(t) \mathbf{L}_G^T$  is distributed according to the Wishart distribution w.p.  $bG$  and  $d$  (Eaton, 1990). Here,  $\mathbf{G} = \mathbf{L}_G \mathbf{L}_G^T$ .

Therefore the dynamically-varying covariance matrix  $\Psi(t)$  is:

$$\Psi(t) \sim \mathcal{GWP}(d, \mathbf{G}, k(\cdot, \cdot));$$

see (Wilson and Ghahramani, 2011).  $\square$

So if our interest was in learning the covariance matrix at any time point, given the data at hand, we could proceed to inference here from, in attempt of the learning of the unknown parameters of this  $\mathcal{GWP}$  process given the lookback-data  $\mathbf{D}_{c,t} := \{\ell_{c,t-t_0} - m_{c,t}, \dots, \ell_{c,t-1} - m_{c,t}\}$  that we use. Our learning scheme then would then involve compounding a Tensor-Variate GP and a  $\mathcal{GWP}$ .

While the above would be a delineated route to recover the temporal variation in the correlation structure of time series data (as studied by Wilson and Ghahramani (2011)), in our study, the focus is on high-dimensional data that display discontinuities, and on learning the relationship  $\xi(\cdot)$  between the observable  $\mathbf{V}$  that generates such data, and the system parameter  $\mathbf{S}$ —with the ulterior aim being parameter value prediction. So learning the time-varying covariance matrix  $\Psi(t)$  is not the focus of our method development. We want to learn  $\xi(\cdot)$  given training data  $\mathbf{D}$ , and this reduces to our interest in learning  $\ell_c$  values  $\forall c = 1, \dots, d$ , which again requires making inference on values of the descriptor variables ( $a$  and  $\delta$ ) at each of the  $d$ -directions in the space of  $\mathbf{S}$ , that then feed into  $\ell_c$  given the mean-subtracted lookback data. We discuss details of this route to learning, below.

### 3.2. Our focus on learning using a Compound Tensor-Variate GP, Scalar-Variate GPs

We find inference defined by a sequential sampling from the scalar-variate GPs (for each of the  $d$  directions of input space), followed by that from tensor-variate GP, directly relevant to our interests. Thus our learning involves a Compound tensor-variate and multiple scalar-variate GPs. To abbreviate, we will refer below to such a Compound Stochastic Process, as a “*nested – GP*” model.

We set up the model as one in which each of  $d$  length scale parameters of a covariance kernel of this tensor-variate GP, is a dynamically varying function  $g_{c,\mathbf{x}}(t)$  of descriptor parameters, where only one new value  $\mathbf{x}_c = (a_c, \delta_c)$  of the descriptor parameters is generated at a given iteration, along the  $c$ -th direction in the space that hosts the  $d$ -dimensional system parameter  $\mathbf{S}$ . This function is modelled as a realisation from the  $c$ -th scalar-variate GP, the covariance function of which is kernel parametrised with an SQE kernel that has an amplitude of  $a_c$ , and (length) scale of  $\delta_c$ . Thus, in the current iteration, the current  $c$ -th covariance kernel is parametrised by the current values of these descriptor parameters.

Hereon, we absorb the dependence of the function  $g(\cdot)$  on the direction index, via the descriptor parameters, and refer to this function as  $g_{\mathbf{x}_c}(t)$ .

Our strategy is that at the  $t$ -th iteration, where  $t \geq t_0$ , we sample a new function  $\xi_t(\cdot)$  from the tensor-variate GP—the covariance structure of which is specified in the first block of updating that

is undertaken earlier within that iteration, upon the sampling of values of the parameters  $\ell_1, \dots, \ell_d$ . Recalling that we model  $\ell_c = g_{\mathbf{x}_c}(t)$ , where  $\mathbf{x}_c = (a_c, \delta_c)^T$ , we first update the amplitude  $a_c$  and length scale parameters  $\delta_c$  for each  $c = 1, \dots, d$ . Using these values, we thereafter sample  $\ell_c$  for each  $c$ , to fix the covariance structure of the generative tensor-variate GP, of the high-dimensional function  $\xi(\cdot)$ . Such an ordered sequence of sampling is possible within a Metropolis-within-Gibbs scheme that we propose for our inference (discussed in the next section).

Here  $\ell_c = g_{\mathbf{x}_c}(t) \sim GP(0, k_c(\cdot, \cdot))$ , where  $k_c(\cdot, \cdot)$  is the covariance function of this scalar-variate GP. Thus, the joint probability of the output of functions  $g_{\mathbf{x}_c}(t - t')$ , at  $t' = 1, \dots, t_0$ , is Multivariate Normal. But  $g_{\mathbf{x}_c}(t - t') = \ell_{c,t-t'}$ , where such a functional output is an element of our mean-subtracted current lookback data  $\mathbf{D}_{c,t} := \{\ell_{c,t-t_0} - m_{c,t}, \dots, \ell_{c,t-1} - m_{c,t}\}$ . Thus, probability of the current lookback data  $\mathbf{D}_{c,t}$  given parameters of the  $c$ -th scalar-variate GP, is Multivariate Normal with mean vector  $\mathbf{0}$  and a  $t_0 \times t_0$ -dimensional current covariance matrix  $\mathbf{S}_c^{(t-1)}$  s.t. likelihood is:

$$\mathcal{L}(\mathbf{S}_c^{(t-1)} | \mathbf{D}_{c,t}) = \mathcal{MN}(\mathbf{0}, \mathbf{S}_c^{(t-1)}),$$

where the current covariance matrix

$$\mathbf{S}_c^{(t-1)} := \left[ a_c^{(t-1)} \exp \left( -\frac{(i-j)^2}{2(\delta_c^{(t-1)})^2} \right) \right]; \quad i, j = 1, \dots, t_0.$$

It is noted that all “current” values of dynamically changing parameters in the  $t$ -th iteration are denoted by the label  $t - 1$ , to designate this value as that accepted at the end of the previous iteration, and that the update on this latest accepted value has not yet been accomplished in the  $t$ -th iteration. Indeed, updating of each such parameter is undertaken in the current, i.e. the  $t$ -th iteration, and a proposed value of a parameter in the  $t$ -th iteration is designated the label  $(t\star)$ . If accepted, this proposed value is then considered the currently accepted value.

Thus, in the above definition of the current covariance matrix along the  $c$ -th direction, the current value of  $\mathbf{x}_c$  is used, where such is denoted by  $(a_c^{(t-1)}, \delta_c^{(t-1)})^T$ . To update the amplitude and scale parameters in each of the  $d$  directions, we propose values of these parameters in the  $t$ -th iteration, respectively from a Truncated-Normal density (left-truncated at 0, mean  $a_c^{(t-1)}$ , and experimentally chosen constant variance  $v_a^{(c)}$ ), and a Normal density (mean  $\delta_c^{(t-1)}$ , and experimentally chosen constant variance  $v_\delta^{(c)}$ ), i.e. proposed values of the 2 descriptor variables in the  $t$ -th iteration are:

$$a_c^{(t\star)} \sim \mathcal{TN}(a_c^{(t-1)}, 0, v_a^{(c)}), \quad \forall c = 1, \dots, d,$$

$$\delta_c^{(t\star)} \sim \mathcal{N}(\delta_c^{(t-1)}, 0, v_\delta^{(c)}), \quad \forall c = 1, \dots, d.$$

Thus, at any fixed value (say  $i$ ) of the input variable (i.e. the iteration number), the  $i$ -th diagonal element  $a_c^{(t-i)}$  of the current covariance matrix  $\mathbf{S}_c^{(t-1)}$ , gives the variance of the Normal density that the r.v.  $\ell_c^{(t-i)}$  can be considered to be sampled from. Thus by fixing the value of the input-space variable, (which in this situation is the iteration number), to  $t$ , length scale hyperparameters are

rendered Normal variates. The proposed variance of this Normal distribution that  $\ell_c$  is sampled from, at the  $t$ -th iteration, is the proposed value of the amplitude parameter in this iteration, i.e.  $a_c^{(t\star)}$ . Under a Random Walk paradigm, the mean of this Gaussian distribution is the current value of the  $\ell_c$  parameter. In other words, we model:

$$\ell_c^{t\star} \sim \mathcal{N}(\ell_c^{(t-1)}, a_c^{(t\star)}).$$

This is essentially suggesting an adaptive Random Walk updating scheme for the  $\ell_c$  parameter,  $\forall c = 1, \dots, d$ .

Thus, in this  $t$ -th iteration, if  $t \geq t_0$ , we model the length scale parameters  $\ell_c, c = 1, \dots, d$ —of the tensor-variate GP that generates samples of  $\xi(\cdot)$ —each as a realisation from a distinct scalar-variate GP, the covariance structure of which is kernel-parametrised s.t. these kernel hyperparameters are (amplitude)  $a_c$  and (scale)  $\delta_c, \forall c = 1, \dots, d$ .

#### 4. Inference

We discuss the MCMC-based inference on the unknowns here. To begin with, we will discuss inference for the model in which each of the length scale hyperparameters of the covariance kernel functions, is modelled as a function of iteration number that is considered a realisation from a scalar-variate, zero-mean GP, the covariance matrix of which parametrised by a stationary kernel, thereby prompting the need to learn the two hyperparameters of each such kernel function. This illustrative case is succinctly referred to as the “*nested – GP*” model. To summarise, the unknowns in this *nested – GP* model include

- 1(a) hyperparameters (global amplitude  $a_c$  and correlation length scale  $\delta_c$ ) of the  $c$ -th kernel function that parametrise the covariance matrix of the zero-mean Multivariate Normal likelihood that equivalently represents the joint probability density of  $t_0$  realisations of the  $c$ -th length scale  $\ell_c: c = 1, \dots, d$ . These hyperparameters are relevant at the  $t$ -th iteration, where  $t \geq t_0$ . At such iterations, the updated values of  $a_c$  and  $\delta_c$  for each  $c$  will provide a value for  $\ell_c$  in each iteration. Here  $\ell_1, \dots, \ell_d$  are the unknown correlation length scales of one of the covariance matrices of the  $k$ -th ordered Tensor Normal likelihood that represents the joint probability of  $n$  realisations of the observable  $\mathbf{V}$ , where  $\mathbf{V} = \xi(\mathbf{S})$ , with  $\mathbf{S} \in \mathbb{R}^d$ . For our illustration of the suggested inference, we will assume that only one of the covariance matrices (say  $\Sigma_p$ , where  $p \in \{1, 2, \dots, k\}$ ) of this tensor-normal density is kernel parametrised, so that we need to model only the  $d$  length scale parameters of this matrix, each as a realisation from a scalar-variate GP, with the global amplitude parameter of this kernel, subsumed as a global scale for other covariance matrices that are learnt directly from MCMC. Thus, in this illustration, there are  $2d$  kernel hyperparameters to learn in total:  $a_1, \dots, a_d, \delta_1, \dots, \delta_d$ .

1(b) the correlation length scales  $\ell_1, \dots, \ell_d$  of the kernel function that parametrises  $\Sigma_p$ , at the  $t$ -iteration, where  $t < t_0$ . At such early iterations, the hyperparameters of the kernel function that parametrises  $\Sigma_p$ , are not modelled as realisations of a scalar-variate GP, but are learnt directly using MCMC.

2 distinct elements of other covariance matrices of the tensor-normal density mentioned in the last bullet point, that are learnt directly using MCMC. We use the qualification “distinct” to clarify that we seek only the upper (or lower) triangle of these symmetrical covariance matrices. Let these elements be jointly referred to as  $\{\sigma_q\}_{q=1}^{q_{max}}$ , where  $q_{max}$  is known, given the number of such covariance matrices (out of the total of  $k - 1$  that are not kernel parametrised) that are directly inferred upon by MCMC, and the dimensionality of each such matrix.

We undertake a Metropolis-within-Gibbs strategy to implement the MCMC-based inference. For all iterations with iteration-number  $t \geq t_0$ , we partition the sought unknowns to 2 sets:  $\{a_c, \delta_c\}_{c=1}^d$  and  $\{\sigma_q\}_{q=1}^{q_{max}}$ , and update the first set of unknowns in the first block update, while the second set is updated in the second block update, at the updated values of  $\{a_c, \delta_c\}_{c=1}^d$ . For  $t < t_0$ , we learn  $\ell_1, \dots, \ell_d$  in the first block update and the  $\sigma_q$  parameters in the next. The algorithm for the inference strategy is provided in Section 1 of the Supplementary Material.

If the *nested-GP* model is not invoked at all, i.e., the length scale parameters  $\ell_1, \dots, \ell_d$  of the kernel function of the kernel-parametrised covariance function  $\Sigma_p$  are treated as unknown constants that are learnt directly using MCMC, then updating of the descriptor variables are omitted. In that case, marginals (allowing for 95% HPDs) of  $\sigma_1, \dots, \sigma_{q_{max}}, \ell_1, \dots, \ell_d$  are learnt. On the other hand, when the *nested-GP* model is invoked, with the “lookback time” chosen to be set as  $t_0$  iterations behind the current iteration, then marginals (with 95% HPDs) on  $\sigma_1, \dots, \sigma_{q_{max}}, a_1, \dots, a_d, \delta_1, \dots, \delta_d$  are obtained. We can, in this case, also generate values of  $\ell_1, \dots, \ell_d$  at the end of the first block update (on the  $a_c, \delta_c$  parameters) in every iteration past iteration number  $t_0$ , since the generative GP that  $\ell_c$  is a realisation of, is updated in this block update. Thus, values of  $\ell_1, \dots, \ell_d$  are predicted at every iteration, when this *nested-GP* model is invoked.

## 5. Application

We illustrate our method using an application on astronomical data. In this application, we are going to learn the location of Sun in the 2-dimensional Milky Way disk. The training dataset comprises a set of 2-dimensional velocity vectors of a sample of stars around the Sun, where such velocity vectors are generated via numerical simulations conducted with varying astronomical models of the Galaxy. Given each such astronomical model of the Galaxy, a set of 2-dimensional vectors of this sample of stars is recorded, i.e. the data recorded at each choice of the Galactic model, is a set of  $p = 2$  velocity components of the same  $k = 50$  stars, rendering the data recorded for each choice of

the galactic model, a matrix with  $k = 50$  rows and  $p = 2$  columns. In fact, a total of  $n = 216$  of such Galactic models were chosen, s.t. the full training data is a cuboid comprising  $n = 216$  number of matrices, each of which is  $50 \times 2$ -dimensional. Each such chosen Galactic model corresponds to a choice of a 2-dimensional vector  $\mathbf{S}$  that bears information about the Milky Way features. Then we treat this situation to state that at each value of the  $d = 2$ -dimensional vector-valued input variable  $\mathbf{S} = (S_1, S_2)^T$ , a  $k \times p$ -dimensional ( $50 \times 2$ -dimensional) matrix-valued observable  $\mathbf{V}$  is generated. There are  $n = 216$  such choices of values of  $\mathbf{S}$ , i.e. there are  $n$  design points, and the value of the observable  $\mathbf{V}$  at each of the  $n$  design points, is identifiable. Thus, the training data is  $\mathbf{D} = \{(\mathbf{s}_i, \mathbf{v}_i)\}_{i=1}^n$ .

At the same time, there exists the test data  $\mathbf{v}^{(test)}$  that comprises the  $p = 2$ -dimensional velocity vectors of the same  $k = 50$  number of real stellar neighbours of the Sun, as measured by the Hipparcos satellite (Chakrabarty, 2007). However, we do not know the real Milky Way feature parameter vector  $\mathbf{s}^{(test)}$  at which  $\mathbf{V} = \mathbf{v}^{(test)}$  is realised.

We frame this problem to state that  $\mathbf{V} = \xi(\mathbf{S})$ , and we want to predict the value  $\mathbf{s}^{(test)}$  of  $\mathbf{S}$ , at which  $\mathbf{V} = \mathbf{v}^{(test)}$ , upon learning  $\xi(\cdot)$ , using the training data  $\mathbf{D}$ .

Since we are observing the velocities of stars around the Sun, the observed velocities will be impacted by certain Galactic features. These features include location of the Sun. In other words, the observed velocities of our stellar neighbours, as expressed as the matrix  $\mathbf{v}^{(test)}$  that is the measured test data, can be regarded as resulting from the Galactic features (including the sought solar location) to bear certain values. Put another way, the matrix of the observed velocities  $\mathbf{V}$  is treated to be (functionally) related to the location vector of the Sun  $\mathbf{S}$ , and this way we can write  $\mathbf{V} = \xi(\mathbf{S})$ . The training data  $\mathbf{D}$  then includes  $n$  pairs of values of chosen solar location vector and the stellar velocity matrix observed at this solar location. Thus, the full training data is a 3-dimensional tensor which has the dimensionality of  $m_1 \times m_2 \times n$ . For the  $i$ -th slice of the tensor is a  $m_2 \times m_1$  matrix, which is observed at the location  $\mathbf{s}_i$ ,  $i = 1, \dots, n$ .

Here for  $\mathbf{V} \in \mathbb{R}^{m_1 \times m_2 \times m_3}$  and  $\mathbf{S} \in \mathbb{R}^d$ ,  $\xi : \mathbb{R}^d \longrightarrow \mathbb{R}^{m_1 \times m_2 \times m_3}$ . So, an observer located at the location  $\mathbf{S} = \mathbf{s}_1$  will observe the neighbouring stars to have a velocity matrix that is different from the velocity matrix of the neighbouring stars measured by another observer at  $\mathbf{S} = \mathbf{s}_2$ , and the velocity matrix measured by observer at location  $\mathbf{s}_i$  bears the stamp of this location,  $i = 1, \dots, n$ . We learn this function  $\xi(\cdot)$  using training data  $\mathbf{D}$ .

In (Chakrabarty et al., 2015), the matrix of velocities was vectorised, so that the observable was then a vector. In our case, the observable is  $\mathbf{V}$ —a matrix. By this process of vectorisation, (Chakrabarty et al., 2015) miss out on the opportunity to learn the covariance amongst the columns of the velocity matrix, (i.e. amongst the components of the velocity vector), distinguished from the covariance amongst the rows, (i.e. amongst the stars that are at distinct relative locations with respect to the observer). Our work allows for clear quantification of such covariances. More

importantly, our work provides a clear template for implementing methodology for learning given high-dimensional data that comprise measurements of a tensor-valued observable.

In our application we realise that the location vector of the observer is 2-dimensional, i.e.  $d=2$  since the Milky Way disk is assumed to be 2-dimensional. Also, each stellar velocity vector is also 2-dimensional, i.e.  $m_1=2$ . (Chakrabarty, 2007) generated such training data by first placing a regular 2-dimensional polar grid on a chosen annulus in an astronomical model of the MW disk. In the centroid of each grid cell, an observer was placed. There were  $n$  grid cells, so, there were  $n$  observers placed in this grid, such that the  $i$ -th observer measured the velocities of  $m_{2i}$  stars that landed in her grid cell, at the end of a simulated evolution of a sample of stars that were evolved in this model of the MW disk, under the influence of the feature parameters that mark this MW model. We indexed the  $m_{2i}$  stars by their location with respect to the observer inside the grid cell, and took a stratified sample of  $m_2$  stars from this collection of  $m_{2i}$  stars while maintaining the order by stellar location inside each grid;  $i = 1, \dots, n$ . Thus, each of the observers records a sheet of information that contains the 2-dimensional velocity vectors of  $m_2$  stars, i.e. the training data comprises  $n$ -number of  $m_2 \times 2$ -dimensional matrices, i.e. the training data is a 3-tensor. We call this tensor  $\mathbf{D}^{(2 \times m_2 \times n)}$ . We realise that the  $i$ -th such velocity matrix or sheet, is realised at the observer location  $\mathbf{s}_i$  that is the  $i$ -th design point in our training data. We use  $n=216$  and  $m_2=50$ . The test data measured by the Hipparcos satellite is then the 217-th sheet, except we are not aware of the value of  $\mathbf{S}$  that this sheet is realised at. We clarify that in this polar grid, observer location  $\mathbf{S}$  is given by 2 coordinates: the first  $S_1$  tells us about the radial distance between the Galactic centre and the observer, while the second coordinate of  $S_2$  denotes the angular separation between a straight line that joins the Galactic centre to the observer, and a pre-fixed axis in the MW. This axis is chosen to be the long axis of an elongated bar of stars that lies pivoted at the Galactic centre, as per the astronomical model of the MW that was used to generate the training data.

As mentioned above, the empirical estimate of the mean tensor is obtained, and used as the mean of the Tensor Normal density that represents the likelihood.

Since the data is a 3-tensor (built of  $n$  observations of the  $50 \times 2$ -dimensional matrix-valued observable  $\mathbf{V}$ ), the likelihood is a 3rd-order Tensor Normal distribution, with zero mean tensor (following the removal of the estimated mean) and 3 covariance matrices that measure:

- amongst-observer-location covariance ( $\Sigma_3^{(216 \times 216)}$ ),
- amongst-stars-at-different-relative-position-w.r.t.-observer covariance ( $\Sigma_2^{(50 \times 50)}$ ), and
- amongst-velocity-component covariance ( $\Sigma_1^{(2 \times 2)}$ ).

We perform kernel parametrisation of  $\Sigma_3$ , using the SQE kernel such that the  $jp$ -th element of  $\Sigma_3$  is kernel-parametrised as  $[\sigma_{jp}] = \exp(-(s_j - s_p)^T \mathbf{Q}^{-1} (s_j - s_p))$ ,  $j, p = 1, \dots, 216$ . Since  $\mathbf{S}$  is a 2-dimensional vector,  $\mathbf{Q}$  is a  $2 \times 2$  square diagonal matrix, the elements  $\ell_1$  and  $\ell_2$  of which, represent the the correlation length scales.

Indeed, the “*nonnested – GP*” model of the covariance function suggests the same correlation length scales for all sampled functions from the tensor-variate GP, and this is a simplification. However, this *nonnested – GP* model still implies that the learning of the  $216 \times 216$ -dimensional covariance matrix  $\Sigma_3$ , has been reduced to the learning of 2 length scale parameters  $\ell_1, \ell_2$ . Here the global amplitude of the kernel function is subsumed into the global scale that multiplies the covariance matrix  $\Sigma_1$ , elements of which are learnt directly by MCMC.

Under the *nested – GP* model,  $\ell_c$  is modelled as a dynamically-varying function that is labelled by the  $c$ -dependent descriptor parameters, that is modelled as a realisation from a scalar-variate, zero-mean GP, s.t. the joint probability of  $t_0$ -number of realisations of  $\ell_c$ —obtained over the last  $t_0$  iterations of the Metropolis-within-Gibbs chain—is multivariate normal, with the current covariance matrix  $\mathbf{S}_c^{(t-1)} = [s_{\alpha\beta}^{(c)}] = \left[ a_c \exp\left(-\frac{(\alpha - \beta)^2}{2\delta_c^2}\right) \right]$ ,  $\alpha, \beta = t - t_0, \dots, t - 1$ ,  $c = 1, 2$ . We are free to choose  $t_0$ , and choose it as large as possible, urged to achieve as wide a coverage of the chain’s history as possible, subject to computational constraints—after all, the bigger is  $t_0$ , the larger is the matrix  $\mathbf{S}_c^{(\cdot)}$ , and therefore more computationally challenging is its inversion, that we need to undertake at every iteration of our MCMC-based inference scheme, (see point 3(b) of the algorithm, discussed above). In light of this challenge, we use  $t_0$  to typically be about  $10^2$ , with  $t_0 \leq 200$  in all our experiments. Thus, at each iteration, under the invoked *nested – GP* model, we update  $a_1, a_2, \delta_1, \delta_2$ , and sample a value of each of  $\ell_1$  and  $\ell_2$ , from the updated scalar-variate, zero-mean GP that this parameter is treated as a realisation from. For the 0-th to the  $t_0 - 1$ -th iterations however, the *nested – GP* model is not implemented, and we learn the  $\ell_1$  and  $\ell_2$  parameters only, in the first block update of our Metropolis-within-Gibbs scheme.

$\Sigma_1$  measures covariance amongst the matrices or sheets obtained at distinct components of the velocity vector. As there are only such 2 components, there are 2 such sheets. However, we are not aware of any input variable at which these sheets are realised. Therefore we need to learn the 3 distinct elements of this  $4 \times 4$ -covariance matrix directly from MCMC. We are going to learn the two diagonal elements and one non-diagonal element in the  $\Sigma_1$  matrix. The two diagonal elements will be learnt by our MCMC algorithm directly. However, the non-diagonal element  $\sigma_{12}^{(1)}$  can be written as  $\sigma_{12}^{(1)} = \rho \sqrt{\sigma_{11}^{(1)} \sigma_{22}^{(1)}}$  where  $\rho$  is the correlation amongst these two vertical sheets in the training data on the observable  $\mathbf{V}$ . Thus, instead of learning the  $\sigma_{12}^{(1)}$  directly, we choose to learn the correlation parameter  $\rho$ , using our MCMC algorithm.

The elements of the  $m_2 \times m_2 = 50 \times 50$ -dimensional  $\Sigma_2$  covariance matrix are not learnt by MCMC. Firstly, there is no input space variable that can be identified, at which the  $ij$ -th element of  $\Sigma_2$  can be considered to be realised, where  $i$  and  $j$  are arbitrarily assigned indices of a pair of stars observed in the 50-star-strong sample of stellar neighbours of the Sun, i.e.  $i, j = 1, \dots, 50$ . So, the  $ij$ -th element of  $\Sigma_2$  gives the covariance amongst the  $i$ -th and  $j$ -th,  $216 \times 2$ -dimensional matrices of the 2-dimensional velocity vectors respectively, of the  $i$ -th and  $j$ -th sampled stars, generated in the

astronomical simulation (that generates the training data), at the 216 different chosen values of the Sun's location on the Milky Way disk;  $\forall i, j = 1, \dots, 50$ . Effectively, the 41st star could have been referred to as the 3rd star in this sample, and the vice versa, i.e. there is no meaningful ordering in the labelling of the sampled stars with these indices. Therefore, we cannot use these labels as values of an input space variable, in terms of which, the covariance between the  $i$ -th and  $j$ -th  $216 \times 2$ -dimensional velocity matrices can be kernel-parametrised. One possibility then is to learn elements in the upper (or lower) triangle of  $\Sigma_2$  directly, using MCMC. However, there are  $25 \times 49$  number of such elements, which is too large a number to allow for direct MCMC-based learning. In light of this, we will perform empirical estimation of the elements of  $\Sigma_2$ . So the  $ij$ -th element of  $\Sigma_2$ , i.e. the covariance between the  $216 \times 2$ -dimensional matrix  $\mathbf{V}_i := [v_{pq}^{(i)}]$  of the  $i$ -th and the matrix  $\mathbf{V}_j := [v_{pq}^{(j)}]$  of the  $j$ -th labelled sampled stars, ( $p = 1, \dots, 216; q = 1, 2$ ), is estimated as  $\widehat{\sigma}_{ij}^{(2)}$ , where:

$$\widehat{\sigma}_{ij}^{(2)} = \frac{1}{2-1} \times \sum_{q=1}^2 \left[ \frac{1}{216} \times \left( \sum_{p=1}^{216} (v_{pq}^{(i)} - \bar{v}_q^{(i)}) \times (v_{pq}^{(j)} - \bar{v}_q^{(j)}) \right) \right],$$

where  $\bar{v}_q^{(i)} = \frac{(\sum_{p=1}^{216} v_{pq}^{(i)})}{216}$  is the sample mean of the  $q$ -th column of the matrix  $\mathbf{V}_i = [v_{pq}^{(i)}]$ .

Thus, within the *nonnested-GP* model, from the training data, we have 5 parameters to learn:  $\ell_1, \ell_2, \sigma_{11}^{(1)}, \rho, \sigma_{22}^{(1)}$ , where these parameters are defined as in:

$$\mathbf{Q} = \begin{pmatrix} \ell_1 & 0 \\ 0 & \ell_2 \end{pmatrix}; \Sigma_3 = \begin{pmatrix} \sigma_{11}^{(1)} & \sigma_{12}^{(1)} \\ \sigma_{12}^{(1)} & \sigma_{22}^{(1)} \end{pmatrix}; \rho = \frac{\sigma_{12}^{(1)}}{\sqrt{\sigma_{11}^{(1)} \sigma_{22}^{(1)}}}$$

The likelihood of the training data given the GP parameters is then given as per Equation 2.1:

$$\begin{aligned} \ell(\mathbf{D} | \ell_1, \ell_2, \sigma_{11}^{(1)}, \sigma_{22}^{(1)}, \rho) &= (2\pi)^{-m/2} \left( \prod_{i=1}^3 |\Sigma_i|^{-m/2m_i} \right) \\ &\times \exp(-\|(\mathbf{D} - \hat{\mathbf{M}}) \times_1 \mathbf{A}_1^{-1} \times_2 \hat{\mathbf{A}}_2^{-1} \times_3 \mathbf{A}_3^{-1}\|^2/2). \end{aligned} \quad (5.1)$$

where  $\Sigma_p = \mathbf{A}_p \mathbf{A}_p^T$ ,  $p = 1, 2, 3$  and  $\hat{\mathbf{M}}$  is the empirical estimate of the mean tensor and  $\hat{\Sigma}_2$  is the empirical estimate of the covariance matrix  $\Sigma_2$  such that  $\hat{\Sigma}_2 = \hat{\mathbf{A}}_2 \hat{\mathbf{A}}_2^T$ . Here  $m_3 = 216$ ,  $m_2 = 50$ ,  $m_1 = 2$ , and  $m = m_1 m_2 m_3$ .

This allows us to write the joint posterior probability density of the unknown parameters given the training data  $\mathbf{D}$ . We generate posterior samples from it using MCMC. To write this posterior, we impose non-informative priors  $\pi_0(\cdot)$  on each of our unknowns (Gaussian with wide, experimentally chosen variances, and mean that is the arbitrarily chosen seed value of  $\ell$ ; Jeffry's priors on  $\Sigma_1$ ). The posterior probability density of our unknown GP parameters, given the training data is then

$$\begin{aligned} \pi(\ell_1, \ell_2, \sigma_{11}^{(1)}, \sigma_{22}^{(1)}, \rho | \mathbf{D}) &\propto \\ \ell(\mathbf{D} | \Sigma_1, \Sigma_3) \times \pi_0(\ell_1) \pi_0(\ell_2) \pi_0(\Sigma_1). \end{aligned} \quad (5.2)$$

The results of our learning and estimation of the mean and covariance structure of the GP used to model this tensor-valued data, is discussed below in Section 7.

Within the *nested – GP* model, from the training data, we have 7 parameters to learn:  $a_1, a_2, \delta_1, \delta_2, \sigma_{11}^{(1)}, \rho, \sigma_{22}^{(1)}$ , where the learnt values of  $a_c, \delta_c$ , ( $c = 1, 2$ ) inform on the zero-mean Multivariate Normal joint probability density of  $t_0$  realisations of the length scale parameter  $\ell_c$ . In every iteration, a value of  $\ell_c$  is sampled, from the updated (at the updated  $a_c, \delta_c$  values), scalar-variate GP that is the generative process for  $\ell_c$ .

The joint posterior probability density of the unknown parameters given the training data  $\mathbf{D}$ , under the *nested – GP* model is given by

$$\begin{aligned} \pi(\delta_1, \delta_2, a_1, a_2, \ell_1, \ell_2, \sigma_{11}^{(1)}, \sigma_{22}^{(1)}, \rho | \mathbf{D}) \propto \\ (2\pi)^{-m/2} \left( \prod_{i=1}^3 |\Sigma_i|^{-m/2m_i} \right) \\ \times \exp(-\|(\mathbf{D} - \hat{\mathbf{M}}) \times_1 \mathbf{A}_1^{-1} \times_2 \hat{\mathbf{A}}_2^{-1} \times_3 \mathbf{A}_3^{-1}\|^2/2) \times \prod_{c=1}^2 \frac{1}{\sqrt{\det(2\pi\mathbf{S})}} \exp\left[-\frac{1}{2}(\ell_c^{(t_0)})^T \mathbf{S}^{-1}(\ell_c^{(t_0)})\right] \times \pi_0(\Sigma_1), \end{aligned} \quad (5.3)$$

where  $\ell_c^{(t_0)} := (\ell_c^{(t-t_0)}, \dots, \ell_c^{(t-1)})^T$ , and  $\mathbf{S}_c = \left[ a_c \exp\left[-\frac{(i-j)^2}{2(\delta_c)^2}\right] \right]$ .

We generate posterior samples using MCMC, to identify the marginal posterior probability distribution of each unknown. The marginal then allows for the computation of the 95% HPD.

## 6. Inverse Prediction–2 Ways

The aim of learning all GP parameters, i.e. the generative process that gives rise to the function  $\xi(\cdot)$  (where the observable  $\mathbf{V} = \xi(\mathbf{S})$ ), is to predict the value  $\mathbf{s}^{(test)}$  of the input variable  $\mathbf{S}$ , at which test data on  $\mathbf{V}$  is realised. In the context of our application,  $\mathbf{s}^{(test)}$  is the location vector of the Sun in the Milky Way disk, i.e. it is the location of the observer who observes the velocity matrix of a sample of nearby stars, as included in the test data. This test data  $\mathbf{v}^{(test)}$  is a  $50 \times 2$  matrix that includes measurements of velocities of 50 stars that are neighbours of the Sun. We use two different methods for making inference on  $\mathbf{s}^{(test)} = (s_1^{(test)}, s_2^{(test)})^T$ , in next section.

In one method we learn the GP parameters and  $s_1^{(test)}$  and  $s_2^{(test)}$  simultaneously from the same MCMC chain run using both training and test data. The tensor that includes both test and training data has dimensions of  $217 \times 50 \times 2$ . We call this augmented data  $\mathbf{D}^* = \{\mathbf{v}_1, \dots, \mathbf{v}_{50}, \mathbf{v}^{(test)}\}$ , to distinguish it from the training data  $\mathbf{D}_V$  that contains only information on  $\mathbf{V}$  measurements. This 217-th sheet of (test) data is realised at the unknown value  $\mathbf{s}^{(test)}$  of  $\mathbf{S}$ , and upon its addition, the updated covariance amongst the sheets generated at the different values of  $\mathbf{S}$ , is renamed  $\Sigma_1^*$ , which is now rendered  $217 \times 217$ -dimensional. Then  $\Sigma_1^*$  includes information about  $\mathbf{s}^{(test)}$  via the SQE-based kernel parametrisation discussed in Section 2.1. The effect of the inclusion of the test data on the other covariance matrices is less; we refer to them as (empirically estimated)  $\hat{\Sigma}_2^*$  and  $\Sigma_3^*$ .

The updated (empirically estimated) mean tensor is  $\hat{\mathbf{M}}^*$ . The likelihood for the augmented data is:

$$\ell(\mathbf{D}^* | \mathbf{s}^{(test)}, \Sigma_1^*, \Sigma_3^*) = (2\pi)^{-m/2} \left( \prod_{i=1}^3 |\Sigma_i^*|^{-m/2m_i} \right) \times \exp \left[ -\|(\mathbf{D}^* - \hat{\mathbf{M}}^*) \times_1 (\mathbf{A}_1^*)^{-1} \times_2 (\hat{\mathbf{A}}_2^*)^{-1} \times_3 (\mathbf{A}_3^*)^{-1}\|^2/2 \right] \quad (6.1)$$

where  $\hat{\mathbf{A}}_2^*$  is the square root of  $\hat{\Sigma}_2^*$ . Here  $m_1 = 217$ ,  $m_2 = 50$ ,  $m_3 = 2$ , and  $m = m_1 m_2 m_3$ . Here  $\mathbf{A}_1^*$  is the square root of  $\Sigma_1^*$  and depends on  $\mathbf{s}^{(test)}$ .

The posterior of the unknowns given the test+training data is:

$$\begin{aligned} \pi(s_1^{(test)}, s_2^{(test)}, \Sigma_1^*, \Sigma_3^* | \mathbf{D}^*) \propto \\ \ell(\mathbf{D}^* | s_1^{(test)}, s_2^{(test)}, \Sigma_1^*, \Sigma_3^*) \times \\ \pi_0(s_1^{(test)}) \pi_0(s_2^{(test)}) \pi_0(q_2^{(*)}) \pi_0(q_1^{(*)}) \pi_0(\Sigma_3^*) \end{aligned} \quad (6.2)$$

As discussed above, we use non-informative priors on all GP parameters and uniform priors on  $s_1^{(test)}$  and  $s_2^{(test)}$ . So  $\pi_0(s_p^{(test)}) = \mathcal{U}(l_p, u_p)$ ,  $p = 1, 2$ , where  $l_p$  and  $u_p$  are chosen depending on the spatial boundaries of the fixed area of the Milky Way disk that was used in the astronomical simulations of (Chakrabarty, 2007). Recalling that the observer is located in a two-dimensional polar grid, (Chakrabarty, 2007) set the lower boundary on the value of the angular position of the observer to 0 and the upper boundary is  $\pi/2$  radians, i.e. 90 degrees, where the observer's angular coordinate is the angle made by the observer-Galactic centre line to the long-axis of the elongated Galactic bar made of stars that rotates pivoted at the Galactic centre (discussed in Section 1). The observer's radial location is maintained within the interval [1.7, 2.3] in model units, where the model units for length are related to galactic unit for length, as discussed in Section 7.4.

In the second method, we infer  $\mathbf{s}^{(test)}$  by sampling from the posterior of  $\mathbf{s}^{(test)}$  given the test+training data and the modal values of the parameters  $q_1, q_2, \sigma_{11}^{(1)}, \rho, \sigma_{22}^{(1)}$  that were learnt using the training data. The modal value of  $\Sigma_3$ , learnt using  $\mathbf{D}$  alone is  $[(\sigma_3^{(M)})_{jp}]_{j=1:p=1}^{217,217}$ , where  $\Sigma_3^* = (\sigma_3^{(M)})_{jp} = \left[ \exp \left( -(\mathbf{s}_j - \mathbf{s}_p)^T \mathbf{Q}^{(M)} (\mathbf{s}_j - \mathbf{s}_p) \right) \right]$ , with the unknown  $\mathbf{s}_{217} = \mathbf{s}^{(test)}$  and the diagonal elements of  $\mathbf{Q}$  given as the modal values  $q_1^{(M)}$  and  $q_2^{(M)}$  that were learnt using training data alone. Similarly,  $\Sigma_1$  is retained as the modal value  $\Sigma_1^{(M)}$  that was learnt using the training data alone. The posterior of  $\mathbf{s}^{(test)}$ , at learnt (modal) values is then

$$\begin{aligned} \pi(s_1^{(test)}, s_2^{(test)} | \mathbf{D}^*, \Sigma_1^{(M)}, \Sigma_3^{(M)}) \propto \\ \ell(\mathbf{D}^* | s_1^{(test)}, s_2^{(test)}, \Sigma_1^{(M)}, \Sigma_3^{(M)}) \times \pi_0(s_1^{(test)}) \pi_0(s_2^{(test)}) \\ \times \pi_0(q_2^{(M)}) \pi_0(q_1^{(M)}) \pi_0(\Sigma_3) | \mathbf{V}^*). \end{aligned} \quad (6.3)$$

where  $\ell(\mathbf{D}^* | s_1^{(test)}, s_2^{(test)}, \Sigma_1^*, \Sigma_3^*)$  is as given in Equation 5.1, with  $\Sigma_3^*$  replaced by  $\Sigma_3$ , and  $\Sigma_1$  replaced by its modal value  $\Sigma_1^{(M)}$ . The priors on  $s_1^{(test)}$  and  $s_2^{(test)}$  are as discussed above. For all parameters, we use Normal proposal densities that have experimentally chosen variances.

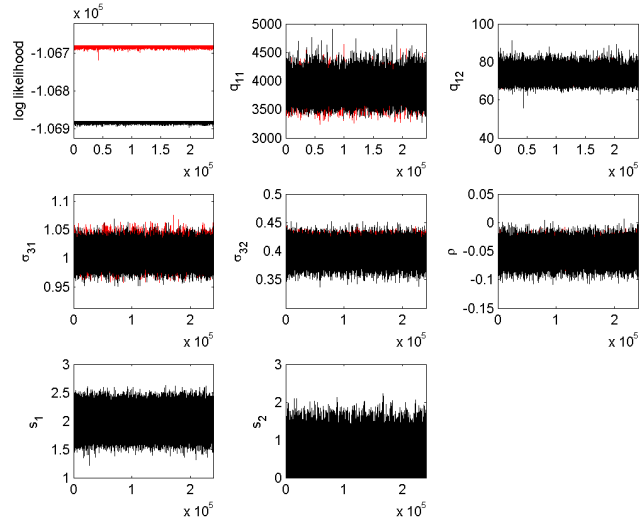


FIG 1. Results from run done with training data  $\mathbf{D}$  with the nonnested – GP model, are shown in grey (or red in the electronic copy of the thesis) while results from run undertaken with training and test data,  $\mathbf{D}^*$ , in this nonnested – GP model, are depicted in black. Traces of the logarithm of the likelihood are displayed from the two runs in the top left panel. Reciprocal of the length scale parameters are the shown in the top middle and right panels; here  $q_c = \ell_c^{-1}$ ,  $c = 1, 2$ . Traces of the learnt diagonal elements  $\sigma_{11}^{(1)}$  and  $\sigma_{22}^{(1)}$ , of the covariance matrix  $\Sigma_1$ , are shown in the mid-row, left and middle panels. Trace of the correlation  $\rho = \frac{\sigma_{12}}{\sqrt{\sigma_{11}^{(1)} \sigma_{22}^{(1)}}}$  is displayed in the mid-row right panel. Prediction of the values of the input parameter  $\mathbf{S} = (S_1, S_2)^T$  is possible only in the run performed with both training and test data. Traces of  $S_1$  and  $S_2$  values learnt via MCMC-based sampling from the joint of all unknown parameters given  $\mathbf{D}^*$ , are shown in the lower panel.

## 7. Results

In this section, we present the results of learning the unknown parameters of the 3rd-order tensor-normal likelihood, given the training as well as the training+test data.

While Figure 1 and Figure 2 depict results obtained from using the *nonnested – GP*, in the following figures, results of the learning of all relevant unknown parameters, using the *nested – GP* model, are included. In this model, the covariance matrix  $\Sigma_3$  (that bears information about the covariance structure between sheets of data generated at different values of the input variable  $\mathbf{S} = (S_1, S_2)^T$ ), is parameterised using a kernel, each length-scale hyperparameter of which, is itself modelled as a dynamically-varying function that is considered sampled from a GP. For each such scalar-variate GP that generates the length-scale  $\ell_c$ ,  $c = 1, \dots, d = 2$  the covariance matrix is itself kernel-parametrised using a stationary kernel, with an amplitude parameter value  $a_c$  and length-scale parameter  $\delta_c$ . Figures that depict results from the *nested – GP* approach will then include results of the learning of amplitude  $a_c$  and smoothing parameters  $d_c := 1/\delta_c$  parameters. Also, our modelling under the *nested – GP* paradigm relies on a lookback-time  $t_0$  which gives the number of iterations over which we gather the generated  $\ell_c$  values.

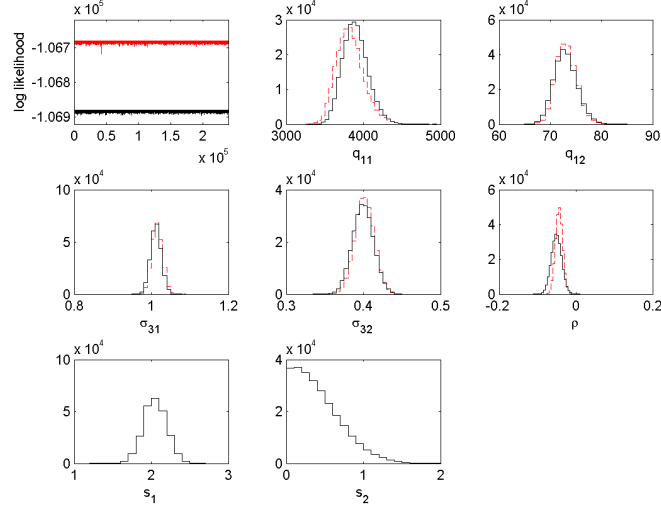


FIG 2. Same as in Figure 1, except the histograms presented here represent histograms of the marginal posterior probability distributions of a parameter given training data  $\mathbf{D}$  (in grey broken lines—or red broken lines, in the electronic version), and given test+training data  $\mathbf{D}^*$  in black solid lines.

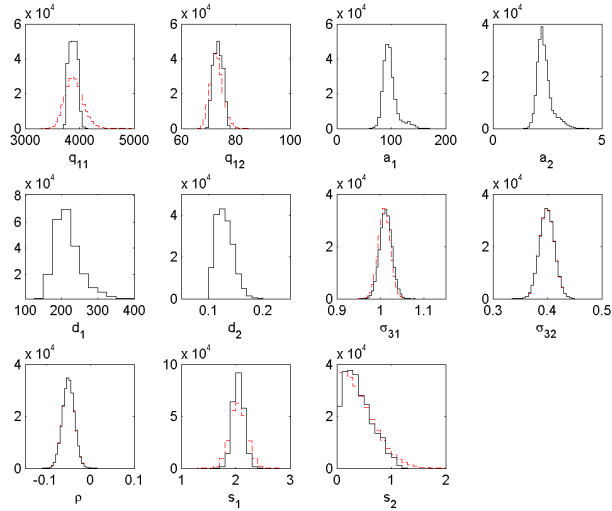


FIG 3. Results from run done with test+training data  $\mathbf{D}^*$  within the nested—GP model, shown in black, as distinguished from the results of learning given the same data, and the nonnested—GP model depicted in grey (or red in the electronic copy of the thesis). Here the used value of  $T_0$  is 200 iterations. Histograms approximating the marginal posterior probability densities of each sought unknown is depicted. Here  $d_c$  is defined as the value of the reciprocal of  $\delta_c$ . Indeed, sought hyperparameter values  $a_c$  and  $\delta_c$  are relevant only to the nested—GP model ( $c = 1, 2$ ). Here, we have undertaken sampling from the joint posterior of all parameters, including the input parameter values  $s_1^{(test)}$  and  $s_2^{(test)}$ , at which the test data are realised. Histograms approximating marginal posterior of each learnt unknown are presented.

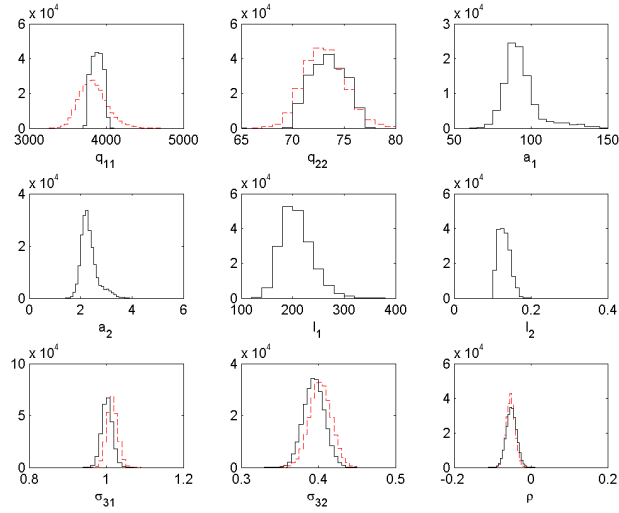


FIG 4. Same as in Figure 3, except that here we present results from run done with only training data  $\mathbf{D}$  within the nested – GP model, shown in black, as distinguished from the results of learning given the same data, and the nonnested – GP model depicted in grey (or red in the electronic copy of the thesis). Given the data used here,  $s_1^{(test)}$  and  $s_2^{(test)}$ , are not learnt here.

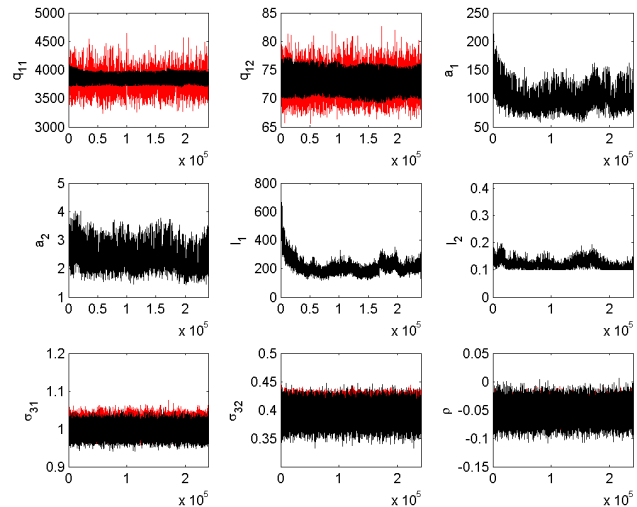


FIG 5. Same as in Figure 4, except that here we present traces of learnt parameters. Traces of parameters learnt within the nonnested – GP model are in grey (or red in the e-version) while the traces obtained using the nested – GP model are shown in black.

### 7.1. Effect of discontinuity in the data, manifest in our results

One difference between the learning of parameters from the *nested* – GP, as distinguished from the *nonnested* – GP models is the quality of the inference, in the sense that the uncertainty of parameters (i.e. the 95% HPDs) learnt using the *nested* – GP models, is less than that learnt using the *nonnested* – GP models. This difference in the learnt HPDs is most marked for the learning of values of  $Q_1$  and  $S_1$ , and  $S_2$  to a lesser extent.

We now attempt explaining this, by invoking the discontinuity in the data, the kernel-parametrised (as a function of  $\mathbf{S}$ ) covariance matrix ( $\boldsymbol{\Sigma}_3$ ) of the distribution of which, is affected by a sharply discontinuous probability distribution of  $S_1$ , and a less sharp discontinuity in the distribution of  $S_2$ . We refer to Figure 8 of Chakrabarty (2007), page 152 (that corresponds to the base astronomical model used in the simulations that generate the training data that we employ), in evidence; the figure is on <https://www.aanda.org/articles/aa/pdf/2007/19/aa6677-06.pdf> This figure informs on the distribution of location  $\mathbf{S}$ , by compatibility of the stellar velocity matrix  $\mathbf{v} = \boldsymbol{\xi}(\mathbf{s})$  realised (in astronomical simulations) at an  $\mathbf{s}$ , to the test velocity matrix  $\mathbf{v}^{(test)}$  (recorded by the *Hipparcos* satellite). In fact, this figure is a contour plot of the distribution of such a compatibility parameter, in the space  $\mathcal{D}$ —where  $\mathbf{S} \in \mathcal{D} \subset \mathbb{R}^2$ ; here the two components of  $\mathbf{S}$  are represented in polar coordinates, with  $S_1$  the radial and  $S_2$  the angular component. We see clearly from this figure, that the distribution across  $S_1$  is highly discontinuous, at given values of  $S_2$  (i.e. at fixed angular bins). In fact, this distribution is visually more discontinuous, than the distribution across  $S_2$ , at given values of  $S_1$ , i.e. at fixed radial bins (each of which is represented by an arcs between two bounding radii). In other words, the velocity matrices that are astronomically simulated at different  $\mathbf{S}$  values, are differently compatible with a give reference velocity matrix ( $\mathbf{v}^{(test)}$ )—and, this difference is discontinuous across values of  $\mathbf{S}$ . Thus, this figure brings forth the discontinuity in the training data, with the input-space variable  $\mathbf{S}$ .

Then, it is incorrect to use a stationary kernel to parametrise the covariance  $\boldsymbol{\Sigma}_3$ , that informs on the covariance between velocity matrices generated at different values of  $\mathbf{S}$ . Our implementation of the *nested* – GP model tackles this shortcoming of the model. However, when we implement the *nonnested* – GP model, the inferential algorithm (Metropolis) needs to explore a wider volume of the state space to accommodate parameter values, given the data at hand—and even then, there is a possibility for incorrect inference under the stationary kernel model. This explains the noted trend of higher 95% HPDs on most parameters learnt using the *nonnested* – GP model, compared to the *nested* – GP model, as observed in comparison of results from runs done with training data alone, or both training and test data (i.e. when prediction from the joint posterior of all parameters give all data is undertaken, to learnt  $\mathbf{s}^{(test)}$ ); see Figure 3, Figure 5, Figure 5. Indeed, this also explains the bigger difference noted in these figures when we compare the learning of  $q_1$  over  $q_2$ , in runs that use the stationary model, as distinguished from the non-stationary model. After all, the discontinuity

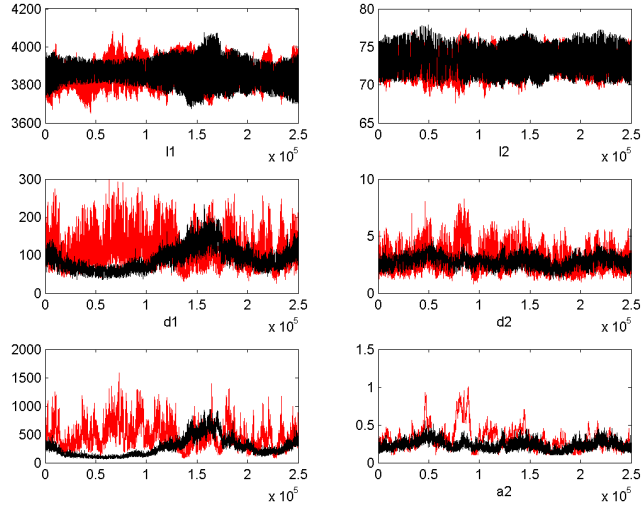


FIG 6. Comparison of traces of unknown smoothness parameters of  $\Sigma_3$  and hyperparameters of GPs invoked to model these parameters, obtained in runs performed with training data  $\mathbf{D}$  and  $t_0 = 50$  (in grey, or red in the e-version) and  $t_0 = 100$  (in black).

across  $S_1$  is discussed above, to be higher than across  $S_2$ .

### 7.2. Effect of varying lookback times, i.e. length of historical data

To check for the effect of the lookback time  $t_0$ , we present traces of the kernel parameters and hyperparameters learnt from runs undertaken within the *nested-GP* model, but different  $t_0$  values of 50 and 100, in Figure 6, which we can compare to the traces obtained in runs performed under the *nested-GP* model, with  $t_0 = 200$ , as displayed in Figure 5.

It is indeed interesting to note the trends in traces of the smoothness, i.e. the reciprocal of  $\ell$  parameters, and values of the amplitude ( $a_1, a_2$ ) and values of smoothing hyperparameters ( $d_1 = 1/\delta_1, d_2 = 1/\delta_2$ ), evidenced in Figure 6 and the results in black in Figure 5. We note the increase in the amplitude of the fluctuations in the traces of these hyperparameters with decreasing  $t_0$ . For smaller values of lookback time  $t_0$ , the average covariance between  $g_{\mathbf{x}_c}(t_1)$  and  $g_{\mathbf{x}_c}(t_2)$  is higher than when  $t_0$  is higher, where the averaging is performed over a  $t_0$ -iteration long interval that has its right edge on the current iteration; here  $\mathbf{x}_c = (a_c, \delta_c)^T$ ,  $c = 1, 2$  and as introduced above, we model the length scale parameter of the kernel that parametrises  $\Sigma_3$ , as  $\ell_c = g_{\mathbf{x}_c}(t)$ . Here  $g_{\mathbf{x}_c}(\cdot)$  is modelled as a realisation from a scalar-variate GP with covariance kernel that is itself kernel-parametrised using an SQE kernel with amplitude  $a_c$  and correlation-length  $\delta_c$ . Then higher covariances between values of  $g_{\mathbf{x}_c}(\cdot)$  at different  $t$ -values in general would suggest higher values of the global amplitude of this parametrised kernel, and higher values of the length-scales of this SQE kernel.

A very interesting trend noted in the parameter traces presented in Figure 6 for  $t_0 = 50, 100$ , and

to a lesser extent for  $t_0 = 200$ , in the results in black in Figure 5, is the global near-periodic existence of crests and troughs in these traces. This periodic fluctuation is more marked for smoothness  $q_1$  ( $=1/\ell l_1$ ) and the hyperparameters of the scalar-variate GP used to model  $g_{\mathbf{x}_1}(\cdot)$ , than for  $q_2$  (and  $a_2$  and  $\delta_2$ ). Let us first seek an explanation for this observed global periodic trend—which is a difficult undertaking in itself, and then explore comparison of the strength of this periodicity across different sets of parameters.

Above, we have convinced ourselves of the fact that the covariance ( $\Sigma_3$ ) amongst velocity slices simulated (astronomically) at different  $\mathbf{S}$  values, is incorrectly parametrised with a stationary kernel, and that a non-stationary kernel is required to model such covariance. We implement such non-stationarity by kernel parametrising  $\Sigma_3$  using a kernel, the length-scales  $\ell_c$  of which is itself stochastic—this stochasticity is generated by a scalar-variate GP according to our model. At any given iteration of our inference scheme, the said model is informed by invoking the past  $t_0$  realisations from such a stochastic process. Then, loosely speaking, the value of  $\ell_c$  in any iteration, is a moving average over the values indicated over this  $t_0$ -iterations wide window—and such a moving average will manifest the result of superposition of the different (discontinuous) modal neighbourhoods present in the data. The more multimodal the data, i.e. larger the number of “classes” (by correlation-length scales) of functional form  $\xi(\cdot)$  sampled from the tensor-variate GP, s.t. superposition of the sample paths will cause a washing-out of the effect of the different modes, and a less prominent global trend will be manifest in the traces. However, for data that is globally bimodal, the superposition of the two “classes” of sampled functions  $\xi(\cdot)$  will create a periodicity in the global trend of the generated  $\ell_c$  values (and thereby of the smoothness parameter values  $q_c$ , where  $q = \ell_c^{-1}$ ).

Again, the larger the value  $t_0$  of the lookback-time parameter, the moving average is over a larger number of samples, and hence greater is the washing-out effect. In fact, depending on the discontinuity in the data, it is anticipated that there is a range of optimal lookback-time values, s.t. the global periodicity is most marked. Thus, the trace of  $q_1$  at  $t_0 = 100$  displays the global periodicity more strongly than that at  $t_0 = 200$  (see Figure 6 and Figure 5). At the same time, the expected higher amplitude in the trace of  $q_1$  with decreasing  $t_0$ , also makes the visual identification of this trend more difficult at lower, than at higher  $t_0$ ; this is clear in the comparison of the trends of the trace of  $q_1$  generated at  $t_0=50$ , as compared to  $t_0=100$  (see Figure 6).

Another point is that the strength this global periodicity will be stronger for the correlation-length scale along that direction in input-space, the discontinuity along which is stronger. Indeed, as we have discussed above, the discontinuity in the data along  $S_1$  is anticipated to be higher than along  $S_2$ . So we would expect a more prominent periodic trend in the trace of  $q_1$  than  $q_2$ . This is indeed what to note in Figure 6. A simulation study can be undertaken to explore the effects of empirical discontinuities.

The arguments above qualitatively explain the observed trends in the traces of the hyperpa-

rameters, obtained from runs using different  $t_0$ . That in spite of discrepancies in  $a_c$  and  $\delta_c$ , with  $t_0$ , values of the length scale parameter  $\ell_c$  (and therefore its reciprocal  $q_c$ ) are concurrent within the 95% HPDs, is testament to the robustness of inference. Stationarity of the traces betrays the achievement of convergence of the chain.

95% HPD credible regions computed on each learnt parameter given the *nonnested-GP* model, are displayed in Table 1. Again, a similar set of results from the chains run with the *nested-GP* models are displayed in Table 2.

TABLE 1  
95% HPD credible regions on each learnt parameter, from the nonnested – GP model

Parameters	using only training data	sampling from posterior predictive	sampling from joint
$q_1$	[3492.1,4198.1]		[3573.2,4220.8]
$q_2$	[68.92,76.88]		[68.37,77.33]
$\sigma_{11}^{(1)}$	[0.9837,1.0380]		[0.9797,1.0338]
$\rho$	[-0.0653,-0.0275]		[-0.0798,-0.0261]
$\sigma_{22}^{(1)}$	[0.3747,0.4234]		[0.3703,0.4237]
$s_1$	-	[1.8212,2.1532]	[1.8038,2.1960]
$s_2$	-	[0.0421,1.2052]	[0.0157,1.2172]

TABLE 2  
95% HPD credible regions on each learnt parameter, from the nested – GP model

Parameters	$t_0 = 200$	$t_0 = 100$	$t_0 = 50$
$q_1$	[3740.96, 3917.32]	[3710.4, 4011.66]	[3650.92, 4033.51]
$q_2$	[70.34, 75.70]	[70.42, 76.43]	[68.94, 76.22]
$a_1$	[78.67, 124.02]	[43.82, 167.35]	[48.27, 219.37]
$a_2$	[1.88, 3.03]	[2.12, 3.57]	[1.64, 6.16]
$d_1$	[155.64, 301.65]	[78.47, 521.67]	[123.42, 828.37]
$d_2$	[0.10, 0.15]	[0.12, 0.46]	[0.10, 0.52]
$\sigma_{31}$	[0.97, 1.02]	[0.97, 1.03]	[0.98, 1.02]
$\sigma_{32}$	[0.37, 0.41]	[0.37, 0.41]	[0.38, 0.41]
$\rho$	[-0.076, -0.031]	[-0.073, -0.03]	[-0.075, -0.032]
$s_1$	[1.83, 2.16]	[1.77, 2.22]	[1.76, 2.24]
$s_2$	[0.138, 1.15]	[0.112, 1.16]	[0.071, 1.15]

We notice that the reciprocal correlation length scale  $q_1$  is a couple of orders of magnitude higher than  $q_2$ ; correlation between values of the sampled function  $\xi(\cdot)$ , at 2 different  $S_1$  values (at the same  $s_2$ ), then wanes more quickly than correlation between sampled functions computed at same  $s_1$  and different  $S_2$  values. Here  $\mathbf{s} = (s_1, s_2)^T$  and given that  $\mathbf{S}$  is the location of the observer who observes the velocities of her neighbouring stars on a two-dimensional polar grid,  $S_1$  is interpreted as the radial coordinate of the observer's location in the Galaxy and  $S_2$  is the observer's angular coordinate. Then it appears that the velocities measured by observers at different radial coordinates, but at the same angle, are correlated over shorter radial-length scales than velocities measured by observers at the same radial coordinate, but different angles. This is understood to be due to the astro-dynamical influences of the Galactic features included by (Chakrabarty, 2007) in the simulation that generates the training data that we use here. This simulation incorporates the joint dynamical effect of the Galactic spiral arms and the elongated Galactic bar (made of stars) that rotate at different frequencies (as per the astronomical model responsible for the generation

of our training data), pivoted at the centre of the Galaxy. An effect of this joint handiwork of the bar and the spiral arms is to generate distinctive stellar velocity distributions at different radial (i.e. along the  $S_1$  direction) coordinates, at the same angle ( $s_2$ ). On the other hand, the stellar velocity distributions are more similar at different  $S_2$  values, at the same  $s_1$ . This pattern is borne by the work by (Chakrabarty, 2004), in which the radial and angular variation of the standard deviations of these bivariate velocity distributions are plotted. Then it is understandable why the correlation length scales are shorter along the  $S_1$  direction, than along the  $S_2$  direction.

Furthermore, for the correlation parameter  $\rho$ , physics suggests that the correlation will be zero among the two components of a velocity vector. These two components are after all, the components of the velocity vector in a 2-dimensional orthogonal basis. However, the MCMC chain shows that there is a small (negative) correlation between the two components of the stellar velocity vector.

### 7.3. Predicting $s^{(test)}$

In the first method, we perform posterior sampling using Metropolis-Hastings, from the joint posterior probability density of all parameters (GP parameters as well as solar location vector), given test+training data. In Figure 1 and Figure 2, we present respectively, traces and histogram-representations of marginal posterior probability densities of the solar location coordinates  $s_1^{(test)}$ ,  $s_2^{(test)}$ ;  $q_1^*$  and  $q_2^*$  that get updated once the test data is added to augment the training data, and parameters  $\sigma_{11}^{1*}$ ,  $\sigma_{22}^{1*}$  and  $\rho^*$ . 95% HPD credible regions computed on each parameter in this inference scheme, are displayed in Table 1. These figures display these parameters in the *nonnested – GP* model. When the *nested – GP* model is used, histogram-representations of the marginals of the aforementioned parameters, are displayed in Figure 3. We notice that the values of the inverse correlation length scales are almost the same as the values learnt with training data.

Prediction of  $s^{(test)}$  using the *nested – GP* models gives rise to very similar results as when the *nonnested – GP* models are used, (see Figure 3 that compares the marginals of the solar location parameters sampled from the joint of all unknowns, given all data, in *nested – GP* models, against those obtained when *nonnested – GP* models are used).

The marginal distributions of  $s_1^{(test)}$  indicates that the marginal is unimodal and converges well, with modes at about 2 in model units. The distribution of  $s_2^{(test)}$  on the other hand is quite strongly skewed towards values of  $s_2^{(test)} \lesssim 1$  radians, i.e.  $s_2^{(test)} \lesssim 57$  degrees, though the probability mass in this marginal density falls sharply after about 0.4 radians, i.e. about 23 degrees. These values tally quite well with previous work (Chakrabarty et al., 2015). In that earlier work, using the training data that we use in this work, (constructed using the the astronomical model *sp3bar3\_18* discussed by (Chakrabarty et al., 2015)), the marginal distribution of  $s_1^{(test)}$  was learnt to be bimodal, with modes at about 1.85 and 2, in model units. The distribution of  $s_2^{(test)}$  found by (Chakrabarty et al., 2015) is however more constricted, with a sharp mode at about 0.32 radians (i.e. about 20 degrees). We do

notice a mode at about this value in our inference, but unlike in the results of (Chakrabarty et al., 2015), we do not find the probability mass declining to low values beyond about 15 degrees. One possible reason for this lack of compatibility could be that in (Chakrabarty et al., 2015), the matrix of velocities  $\mathbf{V}$  was vectorised, so that the training data then resembled a matrix, rather than a 3-tensor as we know it to be. Such vectorisation could have led to some loss of correlation information, leading to the results of (Chakrabarty et al., 2015).

When we predict  $\mathbf{s}^{(test)}$  using test+training data, at the (modal values of the) GP parameters that are learnt from the training data, we generate samples from the posterior predictive of  $\mathbf{s}^{(test)}$  (Equation 6.3) using Metropolis-Hastings. The results are presented in Table 1.

#### 7.4. Astronomical implications

The radial coordinate of the observer in the Milky Way, i.e. the solar radial location is dealt with in model units, but will need to be scaled to real galactic unit of distance, which is kilo parsec (kpc). Now, from independent astronomical work, the radial location of the Sun is set as 8 kpc.

Then our estimate of  $S_1^{(test)}$  is to be scaled to 8 kpc, which gives 1 model unit of length to be  $\frac{8\text{kpc}}{\text{our estimate of } S_1^{(test)}}$ . Our main interest in learning the solar location is to find the frequency  $\Omega_{bar}$  with which the Galactic bar is rotating, pivoted at the galactic centre, (loosely speaking). Here  $\Omega_{bar} = \frac{v_0}{1 \text{ model unit of length}}$ , where  $v_0 = 220 \text{ km/s}$  (see (Chakrabarty, 2007) for details). The solar angular location being measured as the angular distance from the long-axis of the Galactic bar, our estimate of  $S_2$  actually tells us the angular distance between the Sun-Galactic centre line and the long axis of the bar. These estimates are included in Table 3.

TABLE 3

95% HPD on each Galactic feature parameter learnt from the solar location coordinates learnt using the two predictive inference schemes listed above and as reported in a past paper for the same training and test data.

	95% HPD for $\Omega_{bar}$ (km/s/kpc)	for angular distance of bar to Sun (degrees)
from posterior predictive	[48.11, 57.73]	[4.53, 43.62]
from joint posterior	[48.25, 57.244]	[2.25, 46.80]
from Chakrabarty et. al (2015)	[46.75, 62.98]	[17.60, 79.90]

Table 3 displays the Galactic feature parameters that are derived from the learnt solar location parameters, under the different inference schemes using the *nonnested-GP* model, namely, sampling from the joint posterior probability of all parameters given all data, and from the posterior predictive of the solar location coordinates given all data and GP parameters already learnt from training data alone. The derived Galactic feature parameters are the the bar rotational frequency  $\Omega_{bar}$  in the real astronomical units of km/s/kpc and the angular distance between the bar and the Sun, in degrees. The table also includes results from Chakrabarty et al. (2015), the reference for which is in the main paper.

## 8. Model Checking

One way to check for the model and results, given the data at hand, is to generate data from the learnt model, and then compare this generated data with the observed data. Now, the model that we learn, is essentially the tensor-variate GP that is used to model the functional relationship  $\xi(\cdot)$  between the observable  $\mathbf{V}$  and the input-space parameter  $\mathbf{S}$ . By, saying that we want to generate new data, we imply the prediction of a new value of  $\mathbf{V}$ , given the learnt model of this GP.

This prediction of new datum on  $\mathbf{V}$ , is fundamentally different from the inverse prediction of the value  $\mathbf{s}^{(test)}$  of the input-space parameter  $\mathbf{S}$  that we have undertaken—as discussed above—where the sought  $\mathbf{s}^{(test)}$  is the value of  $\mathbf{S}$  at which test data  $\mathbf{v}^{(test)}$  on  $\mathbf{V}$  is recorded. There is no closed-form solution to the posterior predictive of  $\mathbf{s}^{(test)}$  given the test data and the learnt GP parameters.

In fact, at chosen values of  $\mathbf{S}$ —chosen to be the design points in the training data, for convenience—the covariance function  $\Sigma_3$  of this GP, (modelled as a GP with an estimated mean), is known, given the learnt values of the parameters of the kernel used to parametrise  $\Sigma_3$ . However, in our Bayesian inference, we do not really learn a value of any parameter, but learn the marginal posterior of each unknown parameter, given the data. Thus, in order to pin the value of each element of  $\Sigma_3$ , we identify the parameter value corresponding to a selected summary of this posterior distribution. For example, we could choose to define  $\Sigma_3$  at pairs of known design points  $\mathbf{s}_i$ ,  $\mathbf{s}_j$ , and the modal value of  $\ell_c$ —identified from the marginal posterior of  $\ell_c$  inferred upon, given the data. Here  $i, j \in \{1, \dots, n = 216\}$ . The resulting value of the  $ij$ -th element of  $\Sigma_3$  will then provide one summary, of the covariance between the  $50 \times 2$  stellar velocity matrix  $\mathbf{v}_i$  realised at  $\mathbf{S} = \mathbf{s}_i$ , and  $\mathbf{v}_j$  realised at  $\mathbf{S} = \mathbf{s}_j$ . Similarly, the learnt modal values of the parameters  $\sigma_{11}^{(1)}$ ,  $\sigma_{22}^{(1)}$  and  $\rho$  define one summary of the covariance matrix  $\Sigma_1$  that informs on the covariance between the  $2 \times 216 \times 50$ -dimensional sheets of data on each component of the 2-dimensional stellar velocity vector. Again, other summaries of the parameter values could be used as well, for example, the parameter value identified at the mean of the marginal posterior density of this parameter, as learnt given the training data, is also used.

In this model checking exercise, the unknowns are certain elements of the cuboidally-shaped data comprising the 216 number of  $50 \times 2$ -dimensional stellar velocity matrices generated by astronomical simulation, at chosen design points  $\mathbf{s}_1, \dots, \mathbf{s}_{216}$ , i.e. the 3rd-order tensor  $\mathbf{D}_V := \{\mathbf{v}_1, \mathbf{v}_2, \dots, \mathbf{v}_{216}\}$ . In the first attempt to model checking, we generate all elements of the  $q$ -th such simulated stellar velocity matrix  $\mathbf{v}_q$ , (that is generated at the known design point  $\mathbf{s}_q$ ), i.e. generate values of  $50 \times 2 = 100$  unknown elements of matrix  $\mathbf{v}_q$ . We refer to these unknown elements of  $\mathbf{v}_q$  as  $v_{11}^{(q)}, v_{12}^{(q)}, v_{21}^{(q)}, \dots, v_{50,2}^{(q)}$ . The 3rd-ordered tensor without the  $q$ -th slice, is referred to as  $\mathbf{D}_V^{(-q)} := \{\mathbf{v}_1, \mathbf{v}_2, \dots, \mathbf{v}_{q-1}, \mathbf{v}_{q+1}, \mathbf{v}_{216}\}$ . The joint posterior probability density of the 100 unknowns, at the learnt modal values  $q_1^{(mode)}, q_2^{(mode)}, \sigma_{11}^{(1, mode)}, \sigma_{22}^{(1, mode)}, \rho^{(mode)}$  is

$$\pi(v_{11}^{(q)}, v_{12}^{(q)}, v_{21}^{(q)}, \dots, v_{50,2}^{(q)} | \mathbf{D}_V^{(-q)}) \propto \mathcal{TN}_{2 \times 50 \times 216}(\hat{\mathbf{M}}, \Sigma_1^{(mode)}, \hat{\Sigma}_2, \Sigma_3^{(mode)}),$$

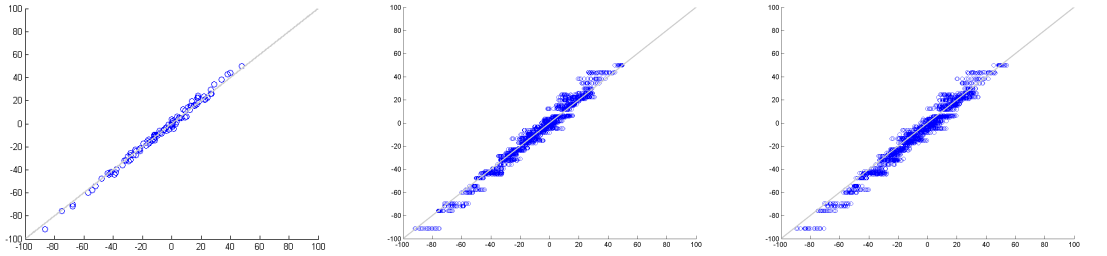


FIG 7. Left: Comparison of the observed and predicted values of elements of the  $q$ -th  $50 \times 2$ -dimensional stellar velocity matrix  $\mathbf{v}_q$ , where 216 such matrices constitute the training data  $\mathbf{D}_V$  (on velocities of 50 stellar neighbours of the Sun) that is generated by astronomical simulations. The predicted or learnt values are obtained from a RW-MCMC chain undertaken with the all elements of the 3rd-order tensor  $\mathbf{D}_V$  known, except for the elements of its  $q$ -th slice, and the learnt values of the parameters of the GP used to model the data at hand, at a chosen summary, namely the mode, of the marginal posterior density of each such learnt GP parameter. Here  $q=200$ . Equality of the observed and predicted values of the elements of  $\mathbf{v}_q$  is indicated by the point lying on the drawn straight line with unit slope; the predicted values are found to lie close to this line. Middle: Depicts a similar comparison, as displayed in the left panel, but for 20 distinct values of  $q$ , namely for  $q = 190, 191, \dots, 210$ . Right: Depicts the same comparison of observed and predicted values of elements of 20 slices  $\mathbf{v}_{190}, \dots, \mathbf{v}_{210}$ , but this time, the employed GP parameters are the means of their respective marginals. Thus, this model-checking exercise checks for the used models and results obtained (given the data at hand) at the mean of the respective posterior.

where,

–the 3rd-ordered tensor-valued data that enters the parametric form of the 3rd-ordered tensor-normal density on the RHS, has elements of its  $q$ -th slice, (out of a total of 216 slices), unknown. All other elements of this  $2 \times 50 \times 216$ -dimensional tensor are known; –uniform priors are used on the unknowns;  $-\Sigma_1^{(mode)}$  is the learnt modal value of the  $2 \times 2$ -dimensional covariance matrix  $\Sigma_1$  s.t. its 1, 1-th element is  $\sigma_{11}^{(1, mode)}$ , 2, 2-th element is  $\sigma_{22}^{(1, mode)}$ , 1, 2-th element is  $\rho^{(mode)} \sqrt{\sigma_{22}^{(1, mode)} \sigma_{11}^{(1, mode)}}$ , and the 2, 1-th element is equal to the 1, 2-th element (as this is a covariance matrix);  $-\Sigma_3^{(mode)}$  is the learnt modal value of the  $216 \times 216$ -dimensional covariance matrix  $\Sigma_3$ , s.t. its  $ij$ -th element is  $\exp \left[ -(\mathbf{s}_i - \mathbf{s}_j)^T \mathbf{Q}^{(mode)} (\mathbf{s}_i - \mathbf{s}_j) \right]$ , with the non-zero elements of the diagonal  $2 \times 2$ -dimensional  $\mathbf{Q}^{(mode)}$ -matrix given by  $q_1^{(mode)}$  and  $q_2^{(mode)}$ .  $\mathbf{s}_i$  being the  $i$ -th design point, is known  $\forall i, j = 1, \dots, 216$ .

To learn the 100 unknowns  $v_{11}^{(q)}, v_{12}^{(q)}, v_{21}^{(q)}, \dots, v_{50,2}^{(q)}$ , we run a RW Metropolis-Hastings chain, with the data defined as above, the known 216 number of design points, and all the learnt, modal parameter values. The joint posterior of the unknowns that defines the acceptance ratio in this chain, is given as in the last equation. The chain is run for 20,000 iterations, for  $q=200$ , and the mean of the last 1000 samples of  $v_{ij}^{(200)}$  is recorded, where  $i = 1, \dots, 50$ ,  $j = 1, 2$ . These sample means  $\bar{v}_{ij}^{(200)}$  then constitute the learnt value of the 100 elements of the 200-th stellar velocity matrix  $\mathbf{v}_{200}$ . We plot the pairs of learnt value  $\bar{v}_{ij}^{(200)}$  of elements of the  $\mathbf{v}_{200}$  matrix, against the empirically observed value of this element,  $\forall i = 1, \dots, 50$ ,  $\forall j = 1, 2$ . The plot is presented in the left panel of Figure 7. Thus, each point on this plot is a pair (empirically observed value of  $v_{ij}^{(200)}, \bar{v}_{ij}^{(200)}$ ), and there are  $50 \times 2 = 100$  points in this plot. The points are found to lie around the straight line with slope 1. In other words, the values of the elements in the  $q$ -th (=200-th) slice of the training data that we learn using our model, are approximately equal to the empirically observed values of these elements. This is corroboration of our models and results.

We attempt a similar prediction of elements of the training data for other values of  $q$ , namely for

$q = 190, \dots, 210$ . The learnt values of elements of  $\mathbf{v}_q$ , for each  $q$ , is plotted against the empirically observed elements of  $\mathbf{v}_q$ . We have superimposed results for all 20 values of  $q$  in the same plot, resulting in the middle panel of Figure 7. Again, the values predicted for all 20 slices, are found to be close to the empirical observations, as betryaed by the points lying close to the straight line of unit slope.

Lastly, we wanted to ensure that the encouraging results from our model checking exercise is robust to changes in the posterior summary of the learnt GP parameters. Thus, we switch to using the mean of the parameter marginal posterior from the posterior mode, and carry out the same exercise of predicting elements of slices  $\mathbf{v}_{190}, \dots, \mathbf{v}_{210}$ . Results are displayed in the right panel of Figure 7. Again, very encouraging corroboration of our used models and results (of learning the GP parameters) is noted. Indeed, in such model checking exercises, encouraging match between the predictions and the empirical observations lends confidence in the used models and results obtained therefrom, given the data at hand—such models and results are the inputs to this exercise. However, if lack of compatibility is noted in such a model checking exercise, between empirical observations and predictions, then it implies that either the used modelling is wrong, and/or the results obtained therefrom given the data are wrong. However, the model checking exercise that we undertake, vindicates our models and results, given the data at hand.

## 9. Conclusions

Our work presents a method for learning tensor-valued functional relations between a system parameter vector, and a tensor-valued observable, multiple measurements of which build up a hypercuboidally-shaped data, that is in general not continuous, thus demanding a non-stationary covariance structure of the invoked GP. We clarify the need for generalising a stationary covariance to one in which the hyperparameters (correlation length scales along each direction of the space of the system parameter vector) need to be treated as dependent on the sample function of the invoked GP. We address this need by modelling the sought tensor-valued function with a tensor-variate GP, each parameter of the covariance function of which, is modelled as a dynamically varying, scalar-valued function that is treated as a realisation from a scalar-variate GP with distinct covariance structure, that we parametrise. We employ Metropolis-within-Gibbs-based inference, that allows comprehensive and objective uncertainties on all learnt unknowns. Subsequent to the learning of the sought tensor-valued function, we make an inverse Bayesian prediction of the system parameter values at which test data on the observable is realised. While in this work we focussed on the learning given discontinuous data, the inclusion of non-stationarity in the covariance is a generic cure for non-stationary data; we will consider an application to a temporally varying, econometric dataset in a future contribution.

## References

Aston, J. A. D., and Kirch, C. (2012), "Evaluating stationarity via change-point alternatives with applications to fMRI data," *Annals of Applied Statistics*, 6(4), 1906–1948.

Barton, T. A., and Fuhrmann, D. R. (1993), "Covariance structures for multidimensional data," *Multidimensional Systems and Signal Processing*, 4(2), 111–123.

Bijma, F., De Munck, J. C., and Heethaar, R. M. (2005), "The spatiotemporal MEG covariance matrix modeled as a sum of Kronecker products," *NeuroImage*, 27(2), 402–415.

Chakrabarty, D. (2004), "Patterns in the Outer Parts of Galactic Disks," *Monthly Notices of the Royal Astronomical Society*, 352, 427.

Chakrabarty, D. (2007), "Phase space structure in the solar neighbourhood," *Astronomy & Astrophysics*, 467(1), 145–162.

Chakrabarty, D., Biswas, M., Bhattacharya, S. et al. (2015), "Bayesian nonparametric estimation of Milky Way parameters using matrix-variate data, in a new Gaussian Process based method," *Electronic Journal of Statistics*, 9(1), 1378–1403.

Chari, R., Coe, B. P., Vucic, E. A., Lockwood, W. W., and Lam, W. L. (2010), "An integrative multi-dimensional genetic and epigenetic strategy to identify aberrant genes and pathways in cancer," *BMC systems biology*, 4(1), 67.

Chari, R., Thu, K. L., Wilson, I. M., Lockwood, W. W., Lonergan, K. M., Coe, B. P., Malloff, C. A., Gazdar, A. F., Lam, S., Garnis, C. et al. (2010), "Integrating the multiple dimensions of genomic and epigenomic landscapes of cancer," *Cancer and Metastasis Reviews*, 29(1), 73–93.

Clarke, R., Ressom, H. W., Wang, A., Xuan, J., Liu, M. C., Gehan, E. A., and Wang, Y. (2008), "The properties of high-dimensional data spaces: implications for exploring gene and protein expression data," *Nature Reviews Cancer*, 8(1), 37.

Dryden, I. L., Bai, L., Brignell, C. J., and Shen, L. (2009), "Factored principal components analysis, with applications to face recognition," *Statistics and Computing*, 19(3), 229–238.

Dunstan, P. K., Foster, S. D., Hui, F. K., and Warton, D. I. (2013), "Finite mixture of regression modeling for high-dimensional count and biomass data in ecology," *Journal of agricultural, biological, and environmental statistics*, 18(3), 357–375.

Eaton, M. L. (1990), "Chapter 8: The Wishart distribution," in *Multi-variate Statistics: A Vector Space Approach* OH: Institute of Mathematical Statistics, pp. 302–333.

Fan, Y. (2017), Statistical Learning with Applications in High Dimensional Data in Health Care Analytics, PhD thesis, University of Maryland.

Fu, X. (2016), Exploring geometrical structures in high-dimensional computer vision data, PhD thesis, University of Otago.

Gramacy, R. (2005), Bayesian treed Gaussian process models, PhD thesis, University of California, SC.

Heinonen, M., Mannerstrm, H., Rousu, J., Kaski, S., and Lhdesmki, H. (2016), Non-Stationary Gaussian Process Regression with Hamiltonian Monte Carlo,, in *Proceedings of the 19th International Conference on Artificial Intelligence and Statistics*, eds. A. Gretton, and C. C. Robert, Vol. 51 of *Proceedings of Machine Learning Research*, PMLR, Cadiz, Spain, pp. 732–740.

Hoff, K. (1997), "Bayesian learning in an infant industry model," *Journal of International Economics*, 43(3-4), 409–436.

Hoff, P. D. et al. (2011), "Separable covariance arrays via the Tucker product, with applications to multivariate relational data," *Bayesian Analysis*, 6(2), 179–196.

Knuth, D. (1997), *The Art of Computer Programming: Seminumerical Algorithms*, Boston, MA, USA: Addison-Wesley Longman Publishing Co.

Kolda, T. G., and Bader, B. W. (2009), "Tensor Decompositions and Applications," *SIAM Review*, 51(3), 455–500.

Leitao, P. J., Schwieder, M., Suess, S., Catry, I., Milton, E. J., Moreira, F., Osborne, P. E., Pinto, M. J., van der Linden, S., and Hostert, P. (2015), "Mapping beta diversity from space: Sparse Generalised Dissimilarity Modelling (SGDM) for analysing high-dimensional data," *Methods in Ecology and Evolution*, 6(7), 764–771.

Manceur, A. M., and Dutilleul, P. (2013), "Maximum likelihood estimation for the tensor normal

distribution: Algorithm, minimum sample size, and empirical bias and dispersion," *Journal of Computational and Applied Mathematics*, 239, 37 – 49.

Mardia, K. V., and Goodall, C. R. (1993), *Spatial-temporal analysis of multivariate environmental monitoring data*, Vol. 6 Elsevier New York.

McCullagh, P. (1987), *Tensor Methods in Statistics* Chapman and Hall.

Oberg, A. L., McKinney, B. A., Schaid, D. J., Pankratz, V. S., Kennedy, R. B., and Poland, G. A. (2015), "Lessons learned in the analysis of high-dimensional data in vaccinomics," *Vaccine*, 33(40), 5262–5270.

Oseledets, I. V. (2011), "Tensor-train decomposition," *SIAM Journal on Scientific Computing*, 33(5), 2295–2317.

Paciorek, C., and Schervish, M. J. (2004), Nonstationary covariance functions for gaussian process regression,, in *In NIPS*, pp. 273–280.

Pang, Y. H., Khor, E. Y., and Ooi, S. Y. (2016), Biometric Access Control with High Dimensional Facial Features,, in *Australasian Conference on Information Security and Privacy*, Springer, pp. 437–445.

Qiang, Q., and Fei, Z. (2011), Generation of Facial Gesture and Expression in High-Dimensional Space,, in *2011 International Conference on Internet Technology and Applications*, pp. 1–5.

Richter, A., Salmi, J., and Koivunen, V. (2008), ML estimation of covariance matrix for tensor valued signals in noise,, in *Acoustics, Speech and Signal Processing, 2008. ICASSP 2008. IEEE International Conference on*, IEEE, pp. 2349–2352.

Sampson, P., and Guttorp, P. (1992), "Nonparametric estimation of nonstationary spatial covariance structure," *Journal of the American Statistical Association*, 87, 108–119.

Sarkar, C. (2015), Improving Predictive Modeling in High Dimensional, Heterogeneous and Sparse Health Care Data, PhD thesis, University of Minnesota.

Schmidt, A., and OHagan, A. (2003), "Bayesian inference for non-stationary spatial covariance structures via spatial deformations," *Journal of the Royal Statistical Society Series B*, 65, 743–758.

Snoek, J., Swersky, K., Zemel, R., and Adams, R. (2014), Input warping for bayesian optimization of non-stationary functions,, in *In ICML*, pp. 1674–1682.

Theobald, D. L., and Wuttke, D. S. (2008), "Accurate structural correlations from maximum likelihood superpositions," *PLoS computational biology*, 4(2), e43.

Tolvanen, V., Jylnki, P., and Vehtari, A. (2014), Expectation propagation for nonstationary heteroscedastic gaussian process regression,, in *IEEE International Workshop on Machine Learning for Signal Processing (MLSP)*, pp. 1–6.

Wang, J. (2011), *Geometric structure of high-dimensional data and dimensionality reduction* Springer.

Wang, W., Chen, L., and Zhang, Q. (2015), "Outsourcing high-dimensional healthcare data to cloud with personalized privacy preservation," *Computer Networks*, 88, 136–148.

Warton, D. I. (2011), "Regularized Sandwich Estimators for Analysis of High-Dimensional Data Using Generalized Estimating Equations," *Biometrics*, 67(1), 116–123.

Werner, K., Jansson, M., and Stoica, P. (2008), "On estimation of covariance matrices with Kronecker product structure," *IEEE Transactions on Signal Processing*, 56(2), 478–491.

Wilson, A., and Ghahramani, Z. (2011), Generalised Wishart Processes,, in *In Proceedings of the Twenty-Seventh Conference Annual Conference on Uncertainty in Artificial Intelligence (UAI-11)*, Corvallis, OregonAUAI Press, pp. 736–744.

Xu, Z., and Yan, F. (2015), "Infinite Tucker Decomposition: Nonparametric Bayesian Models for Multiway Data Analysis," *arXiv:1108.6296*, .

Xu, Z., Yan, F. et al. (2011), "Infinite Tucker decomposition: Nonparametric Bayesian models for multiway data analysis," *arXiv preprint arXiv:1108.6296*, .